Redox Biology 65 (2023) 102831

Contents lists available at ScienceDirect

Redox Biology

journal homepage: www.elsevier.com/locate/redox

Cellular and exosomal GPx1 are essential for controlling hydrogen peroxide balance and alleviating oxidative stress in hypoxic glioblastoma

Fu-Ju Lei [a], Jung-Ying Chiang [b,c], Huan-Jui Chang [b,d], Der-Cherng Chen [e], Hwai-Lee Wang [b], Hsi-An Yang [b], Kai-Yu Wei [b,f], Yen-Chih Huang [b,g], Chi-Chung Wang [h], Sung-Tai Wei [i,1], Chia-Hung Hsieh [a,b,j,*,1]

[a] Graduate Institute of Clinical Medical Sciences, China Medical University, Taichung, Taiwan
[b] Graduate Institute of Biomedical Sciences, China Medical University, Taichung, Taiwan
[c] Department of Neurosurgery, China Medical University Hsinchu Hospital, Hsinchu, Taiwan
[d] School of Medicine, Chung Shan Medical University, Taichung, Taiwan
[e] Department of Neurosurgery, China Medical University and Hospital, Taichung, Taiwan
[f] Mingdao High School, Taichung, Taiwan
[g] Department of Medical Imaging, China Medical University and Hospital, Taichung, Taiwan
[h] Graduate Institute of Biomedical and Pharmaceutical Science, Fu Jen Catholic University, New Taipei, Taiwan
[i] Division of Neurosurgery, Department of Surgery, An Nan Hospital, China Medical University, Tainan, Taiwan
[j] Department of Medical Research, China Medical University Hospital, Taichung, Taiwan

ARTICLE INFO

Keywords:
Tumor hypoxia
Hydrogen peroxide
Glutathione peroxidase 1
Exosomes hypoxia-inducible factor
Glioblastoma

ABSTRACT

Tumor hypoxia promotes malignant progression and therapeutic resistance in glioblastoma partly by increasing the production of hydrogen peroxide (H_2O_2), a type of reactive oxygen species critical for cell metabolic responses due to its additional role as a second messenger. However, the catabolic pathways that prevent H_2O_2 overload and subsequent tumor cell damage in hypoxic glioblastoma remain unclear. Herein, we present a hypoxia-coordinated H_2O_2 regulatory mechanism whereby excess H_2O_2 in glioblastoma induced by hypoxia is diminished by glutathione peroxidase 1 (GPx1), an antioxidant enzyme detoxifying H_2O_2, via the binding of hypoxia-inducible factor-1α (HIF-1α) to GPx1 promoter. Depletion of GPx1 results in H_2O_2 overload and apoptosis in glioblastoma cells, as well as growth inhibition in glioblastoma xenografts. Moreover, tumor hypoxia increases exosomal GPx1 expression, which assists glioblastoma and endothelial cells in countering H_2O_2 or radiation-induced apoptosis *in vitro* and *in vivo*. Clinical data explorations further demonstrate that GPx1 expression was positively correlated with tumor grade and expression of HIF-1α, HIF-1α target genes, and exosomal marker genes; by contrast, it was inversely correlated with the overall survival outcome in human glioblastoma specimens. Our analyses validate that the redox balance of H_2O_2 within hypoxic glioblastoma is clinically relevant and could be maintained by HIF-1α-promoted or exosome-related GPx1.

1. Introduction

Hydrogen peroxide (H_2O_2) is a type of reactive oxygen species (ROS) primarily generated by the mitochondria but also arises as a by-product of different metabolic pathways within cells [1,2]. Its precursor, superoxide anion ($O_2^{\bullet-}$), from mitochondrial complexes I, II, and III or NADPH oxidases (NOXs), is rapidly converted to H_2O_2 by distinct superoxide dismutases (SODs). Compared to other ROS such as $O_2\bullet-$ and hydroxyl radical ($^{\bullet}OH$), H_2O_2 is a non-radical ROS that is relatively less reactive with biomolecules and has a longer biological lifespan (half-life ~ 1 ms). In mammalian cells, H_2O_2 serves as a signaling molecule at low concentrations and regulates various physiological processes, including cell proliferation, differentiation, migration, and metabolism [3,4]. However, excessive production of H_2O_2 can lead to oxidative stress, which can damage cellular macromolecules, such as lipids, proteins, or DNA, and further lead to cell cycle arrest or cell death. Therefore, it is necessary to strictly control its levels through catabolic enzymes such as catalase (CAT) [5], peroxiredoxins (Prx) [6], and glutathione

* Corresponding author. No. 91, Hsueh-Shih Road, Taichung, 404, Taiwan.
E-mail address: chhsiehcmu@mail.cmu.edu.tw (C.-H. Hsieh).
[1] These authors contributed equally to this work.

https://doi.org/10.1016/j.redox.2023.102831
Received 20 June 2023; Received in revised form 25 July 2023; Accepted 26 July 2023
Available online 5 August 2023

peroxidases (GPx) [7]. These enzyme systems maintain cellular redox homeostasis, particularly in response to various stresses or stimuli.

Tumor hypoxia, either chronic or cycling hypoxia, is a prevalent tumor microenvironment that exerts a significant impact on the regulation of H_2O_2 production in solid tumor cells [8]. Hypoxia causes inefficient electron transfer within the electron transport chain at the mitochondria, which enhances the baseline ROS as well as H_2O_2 produced by mitochondria due to the lack of oxygen (O_2) as the electron recipient [9,10]. These ROS further promote Hypoxia-inducible factor-1α (HIF-1α) stabilization and signaling [11,12]. Subsequently, HIF-1α regulates glycolysis-related genes and triggers a switch of energy metabolism from oxidative phosphorylation to glycolysis (Warburg effect) [13]. This leads to inhibiting mitochondrial respiration and H_2O_2 generation, resulting in the hypoxic adaption of tumor cells [14]. However, hypoxia can activate another intracellular source of ROS by regulating NOXs [9]. Increased expression of NOX1, NOX2, NOX4, and NOX5 or their regulatory components has been found in many types of cancers and is associated with malignant progression and poor clinical outcomes. Moreover, tumor hypoxia promotes NOX4 expression via HIF-1α-mediated transactivation of its promoter [15]. This mechanism contributes to tumor hypoxia-induced elevation of H_2O_2 because the main oxidation product of NOX4 is H_2O_2.

Although hypoxia contributes to the production of H_2O_2, it also has a regulatory function in the catabolism of H_2O_2. Upon the occurrence of hypoxia in pulmonary arterial smooth muscle, AMP-activated protein kinase (AMPK) is activated, and forkhead box protein O1 (FoxO1) levels are increased, leading to the induction of CAT expression and activity [16]. Furthermore, during hypoxia and reoxygenation in mouse pulmonary artery smooth muscle cells, GPx1 is protective against mitochondrially generated H_2O_2 [17]. However, whether similar mechanisms of CAT or GPx1 can be observed in tumor hypoxia remains unclear. Unlike CAT and GPx, tumor cells can upregulate the expression of Prx1 or Prx3 in response to hypoxia or reoxygenation [18–21]. The upregulation of Prx under hypoxia is believed to confer a survival advantage on tumor cells by shielding them from the harmful effects of ROS or generating resistance to radiation and chemotherapy. Nevertheless, the mechanisms by which tumor hypoxia mediates the catabolism of H_2O_2 and maintains redox homeostasis remain unclear.

This study aims to explore how tumor hypoxia regulates the equilibrium of H_2O_2 in glioblastoma. Our findings indicate that GPx1 is a dominant enzyme involved in the hypoxic tumor-mediated catabolism of H_2O_2 in glioblastoma. Tumor hypoxia leads to upregulation of GPx1, preventing H_2O_2 overload and apoptosis in glioblastoma cells and xenografts via a HIF1-α–dependent pathway. In addition, exosomes secreted by hypoxic tumor cells contain high levels of GPx1. These exosomal GPx1s contribute to the resistance of oxidative stress and radiation for tumor and endothelial cells *in vitro* and *in vivo*. These results suggest that GPx1, both intracellular and exosomal, plays a critical role in guarding against oxidative stress and providing radiation resistance for glioblastoma in hypoxic tumor microenvironments.

2. Materials and methods

2.1. Cell culture

The human glioblastoma cell line, GBM8401, was acquired from the Bioresource Collection and Research Center (BCRC), while U251 was procured from Sigma-Aldrich. The U251 cells were cultured in Dulbecco's Modified Eagle Medium (DMEM, Life Technologies) supplemented with 10% fetal bovine serum (FBS), 10 mM HEPES, and 1% penicillin-streptomycin (P/S). The GBM8401 cells were maintained in RPMI 1640 (Invitrogen) supplemented with 10% FBS, 10 mM HEPES, and 1% P/S. Primary glioblastoma cells, GBM04T and GBM09T, derived from our previous study [22], were propagated as tumor spheres in serum-free DMEM-F12 supplemented with 2% B27, 20 ng/mL bFGF, and 20 ng/mL EGF. The human umbilical vein endothelial cells (HUVECs) were procured from Sciencell Company and cultured with endothelial cell medium (ECM) (Sigma-Aldrich) containing 5% FBS, 1% endothelial cell growth supplement (ECGS), and 1% P/S.

2.2. In vitro hypoxic treatments

Hypoxic conditions were achieved by incubating the cells in a Biospherix hypoxic chamber. The cells were subjected to *in vitro* non-interrupted hypoxic or cycling hypoxic stress, as previously described [23]. In brief, the cell cultures were subjected to three cycles, each consisting of exposure to 0.5%–1% O_2 for 1 h, interrupted by 5% CO_2 and air for 30 min during cycling hypoxic treatment (Cy.H.), or continuous exposure to 0.5%–1% O_2 for 4 h during non-interrupted hypoxic treatment (C.H.).

2.3. Western blot analysis

The cells were lysed, and the extracts were prepared as previously described [24]. Monoclonal or polyclonal anti-GPx1 (diluted 1:500; Picoband), anti-GPx3 (diluted 1:550; R&D systems), anti–HIF–1α (diluted 1:650; Novus), anti–HIF–2α (diluted 1:450; Novus), anti-CD63 (1:600; GeneTex), anti-CD81 (1:500 dilution; GeneTex), and anti-Calnexin (1:650 dilution; Cell Signaling) antibodies were used to detect GPx1, GPx3, HIF-1α, HIF-2α, CD63, CD81, and Calnexin proteins in cells using 150 μg of cell extract. The western blots were normalized using a monoclonal anti-β-actin antibody (diluted 1:10,000; Sigma-Aldrich), and protein bands were quantified using the ImageJ software.

2.4. Real-time quantitative polymerase chain reaction (Q-PCR)

The cellular RNA was acquired utilizing the RNeasy Minutesi Kit (Qiagen) in accordance with the guidelines provided by the manufacturer. Subsequently, reverse transcription was performed employing the Omniscript RT (Qiagen) system, utilizing random hexamers (Applied Biosystems). Q-PCR analysis was executed according to previously described methods [24]. The primers employed for quantitative evaluation of GPx1, GPx3, and the housekeeping gene 60S acidic ribosomal proteins were as follows: for human GPx1 (NM_000581.4, 143bp), forward primer (F) 5′-TATCGAGAATGTGGCGTCCC-3′ and reverse primer (R) 5′- TCTTGGCGTTCTCCTGATGC -3'; for human GPx3 (NM_001083929.1, 105 bp), (F) 5′-CCATTTGGCTTGGTCATTCTGGG-3′ and (R) 5′-CACCTGGTCGAACATACTTGAGAC-3'; for the housekeeping gene 60S acidic ribosomal protein (NM_016183.4, 150 bp), (F) 5′-ACGAGGTGTGCAAGGAGGGC-3′ and (R) 5′-GCAAGTCGTCTCCCATC TGC-3'.

2.5. Enzyme activity assays of H_2O_2-scavenging enzymes

The catalase assay and glutathione peroxidase assay kits, acquired from Sigma-Aldrich, were employed to assess the intracellular activities of catalase and glutathione peroxidase, respectively, according to the manufacturer's instructions. On the other hand, the intracellular activities of peroxiredoxins were evaluated following a published protocol [25]. To ensure the veracity of our enzyme activity assessments, we incorporated affirmative benchmarks to validate the efficacy of the employed methodology. The catalase assay and glutathione peroxidase assay kits, procured from Sigma-Aldrich, were equipped with pre-included reagents serving as positive controls. Moreover, for the evaluation of peroxiredoxin activity, we acquired purified and functionally active peroxiredoxin from MyBioSource.com. Conversely, the negative controls exclusively consisted of reagents devoid of purified enzymes or cellular extracts.

2.6. Vector constructions and viral transduction

The lentiviral vector pLKO AS2, which was obtained from the National RNAi Core Facility in Taiwan, was used as the foundation for the production of a lentiviral reporter vector. The multiple cloning sites (MCS) of the pTA-Luc vector from Clontech were utilized to insert a cDNA fragment containing the −2000 ~ +1 bp GPx1 promoter to stimulate the expression of the firefly luciferase gene. To create the GPx1 promoter-induced reporter gene cassette, polymerase chain reaction (PCR) was used to amplify the cassette from the promoter to SV40 poly-A on the pTA-Luc vector. This cassette was then integrated into pLKO AS2 to create pLKO AS2-GPx1-p using *Xho*I and *Mlu*I restriction enzymes. The conserved core of hypoxia response element (HRE) in GPx1 promoter was inactivated by the Quick Change Site-directed Mutagenesis Kit from Stratagene (5′-CGTG-3′ to 5′-ATAA-3′). The full-length human GPx1 cDNA without 3′-UTR (609bp; RefSeq: NM_000581.2) was amplified and subcloned into pAS2.EYFP.puro at the *Nhe*I and *Eco*RI sites. The Lenti-luciferase-P2A-Neo vector from Addgene was used to produce glioblastoma reporter cells (U251-luc, GBM04T-luc, and GBM09T-luc) containing EF-1α promoter-driven luciferase (Luc). Lentiviral vectors carrying short hairpin RNA (shRNA) targeting HIF-1α, HIF-2α, and GPx1, as well as scrambled shRNA, were provided by the National RNAi core facility, Academia Sinica in Taiwan. To develop a tetracycline (Tet)-regulatable GPx1 knockdown system, the lentiviral vector pLVCT-tTR-KRAB from Addgene was used to express GPx1 shRNA. Lentivirus production and cell transduction were performed according to established protocols [26]. All constructs were verified by DNA sequencing.

2.7. Promoter analysis and luciferase assays

The hypoxia response element (HRE) present in the proximal promoter region (−2000 to +1) of human GPx1 was obtained from the eukaryotic promoter database (http://epd.vital-it.ch/). To investigate the role of HIF-1α or HIF-2α in hypoxia-induced transcriptional activation of GPx1, GPx1 promoter-driven firefly luciferase reporter-transfected U251 and GBM09T cells were transfected with pcDNA3 control plasmids or pcDNA3-HIF-1α containing an oxygen-dependent degradation domain (ODD) deletion mutant (HIF-1-OD) for 48 h under normoxic conditions. To quantify the impact of HRE mutations on GPx1 promoter reporter activity, the baseline luciferase-expressing vector phRL-SV40, containing the Renilla luciferase gene (Promega), was transfected into constructs of HRE-mutant and wild-type GPx1 promoters before independent transfection into GBM8401, U251, GBM04T, and GBM09T cells. The cells were then treated with or without hypoxia for 24 h, and firefly luciferase activity was measured and normalized to Renilla luciferase activity. The luciferase activity was determined by combining 10 μL of extracts from 1×10^5 cells with 100 μL of luciferase assay reagent (Promega) following the manufacturer's instructions.

2.8. Chromatin immunoprecipitation (ChIP) assay

ChIP assay was conducted using the Imprint Chromatin Immunoprecipitation Kit (Sigma-Aldrich), following the manufacturer's protocol, with an anti–HIF–1α antibody (Novus). Polymerase chain reaction (PCR) was carried out for the HRE in the GPx1 promoter using these specific primers: (F) 5′- GCTCGGGCGCACTCTCCAGCC-3′ and (R) 5′-CCAGCGGAGCGCCCCGAACA-3'.

2.9. Cell viability assay

Cell viability was assessed using the 3-[4,5-dimethylthiazol-2-yl]-2,5 diphenyl tetrazolium bromide (MTT) assay in accordance with the manufacturer's instructions. Cells, at a density of 1×10^5/well, were seeded in 96-well plates containing 0.2 mL of medium per well. After 48 h of treatment, the medium from each well was cautiously aspirated, and the cells were washed 2–3 times with media devoid of FBS. Next, 200 μL of MTT solution (5 mg/mL) was added to each well, and the plates were then incubated for 4 h in a 5% CO_2 incubator to assess cell viability. Following the incubation, the medium was carefully aspirated, and purple formazan crystals were dissolved using dimethyl sulfoxide (DMSO). Subsequently, the 96-well plates were centrifuged at 3500 rpm for 5 min, and 50 μL of the colored media were transferred into a fresh 96-well plate. Finally, absorbance was measured at 570 nm for each well using a SPECTROstar Nano plate reader (BMG Labtech Inc).

2.10. Caspase-3 activity and apoptosis assays

The activities of caspase-3-like proteases were ascertained utilizing the Caspase-3 Colorimetric Activity Assay Kit (Sigma-Aldrich), in accordance with the manufacturer's protocol. To determine cell apoptosis, Annexin V and propidium iodide staining was executed by using the Annexin V-FITC Apoptosis Detection Kit (Sigma-Aldrich) for 10 min at room temperature, as directed by the manufacturer's instructions, followed by flow cytometric analysis.

2.11. Intracellular H_2O_2 and ROS assays

Intracellular levels of H_2O_2 or ROS were assessed using 10-acetyl-3,7-dihydroxyphenoxazine (Amplex Red, Molecular Probes) to evaluate H_2O_2 or carboxy-2′ 7' dihydrodichlorofluorescein diacetate (H2DCFDA, Molecular Probes) to assess total ROS. Cells were incubated in a phenol-free medium in the presence of 50 μM Amplex Red and 0.1 U/mL horseradish peroxidase or 10 μM H2DCFDA under specific treatment conditions. Moreover, cells were incubated with 1 μM of ROS-insensitive probe carboxy-DCFDA (Invitrogen) instead of H2DCFDA for the negative control group. Fluorescence was measured using a SpectraMax M2/M2e Microplate Reader (Molecular Devices) with excitation at 530 nm and emission at 590 nm for Amplex Red, or excitation at 485 nm and emission at 520 nm for H2DCFDA.

2.12. Protein carbonyl assay

The Protein Carbonyl Content Assay Kit (Abcam) was employed to elicit protein carbonyl groups according to the manufacturer's prescribed guidelines. Tumor tissues were homogenized in deionized water (dH_2O) with the aid of a homogenizer. Subsequent to centrifugation, the resulting supernatant was collected, and the samples were diluted with dH_2O to achieve an approximate protein concentration of 10 mg/mL. For each individual sample, 100 μL of DNPH was introduced, followed by vigorous mixing and an incubation period of 10 min at room temperature. Subsequently, 30 μL of Trichloroacetic Acid Solution/TCA was added to each sample, followed by further mixing, placement on ice for 5 min, and centrifugation at maximum velocity for 2 min. The supernatant was meticulously extracted and discarded. Cold acetone (500 μL) was utilized to wash the resulting pellet in each tube, and the sample underwent sonication in a sonicating bath for 30 s. Afterward, the sample was placed at −20 °C for 5 min, subjected to a 2-min centrifugation, and the acetone was cautiously removed. Finally, 200 μL of guanidine solution was introduced to each tube and briefly subjected to sonication. The optical density at approximately 375 nm was measured employing a microplate reader within a 96-well plate.

2.13. Cells irradiation and clonogenic survival assay

Cells were exposed to single doses of X-rays (0–10 Gy) delivered at a rate of 2.85 Gy/min from a high-energy linear accelerator (Varian). Subsequently, the cells were immediately harvested and seeded in 6-well plates for clonogenic survival assay after irradiation. The clonogenic survival assay was conducted following previously described protocols [27]. In brief, irradiated cells were plated in triplicate in

60-mm dishes. After 14 days, colonies were fixed, stained with crystal violet in 50% ethanol, and counted to determine surviving fractions, with colonies containing >50 cells being taken into account.

2.14. Exosome isolation

Exosomes were extracted through a commercially available Exo-Quick exosome precipitation solution (System Biosciences) as per the manufacturer's guidelines. Briefly, cells were seeded in a 10 cm dish and incubated until the cell density reached 80%. Subsequently, the medium (with a minimum volume of 10 mL) was collected and subjected to centrifugation at 3000×*g* for 15 min to eliminate cells and cellular debris. The resulting supernatant was then transferred to a fresh tube, and an appropriate volume of solution (2 mL of precipitation solution per 10 mL of medium) was added. The sample was carefully stored overnight at 4 °C, ensuring the upright placement of the tube and avoiding any rotation or mixing during the incubation period. Afterward, the sample was centrifuged at 1500×*g* for 30 min. The supernatant was discarded, and the remaining solution was meticulously eliminated by spinning down at 1500×*g* for 5 min. The exosome pellet was reconstituted in 100 μL of sterile 1× PBS and promptly utilized for downstream applications.

2.15. Animal models

Six-week-old male BALB/c nu/nu mice, procured from the Animal Facility of the National Science Council, were employed to generate intracranial GBM patient-derived xenografts (PDX) or orthotopic glioblastoma xenografts following previously described methods [28,29]. Specifically, tumor reporter cells (1×10^5 GBM04T-luc, 2×10^5 GBM8401-luc, and 2×10^5 U251-luc cells) with or without Tet-inducible GPx1 shRNA were trypsinized and independently injected into the left basal ganglia of anesthetized mice. All animal studies were carried out under the Institutional Guidelines of China Medical University (Taichung, Taiwan) with the permission of the local Ethical Committee for Animal Experimentation (CMUIACUC-2021-155).

2.16. Animal treatments

To distinguish hypoxic regions within the tumor microenvironment, mice with glioblastoma were intravenously injected with the hypoxia marker, pimonidazole (70 mg/kg, intraperitoneal; HPI), and a perfusion marker, Hoechst 33342 (1 mg/mouse; intravenous; Sigma) 3 h and 1 min, respectively, before tumor excision on day 14 after tumor implantation. To observe the effect of GPx1 knockdown on tumor growth, mice with orthotopic GBM04T-luc xenografts were administered doxycycline (Dox) in their drinking water (100 μg/mL) after tumor implantation. To investigate the role of GPx1 in hypoxic exosome-mediated radiation resistance *in vivo*, mice with orthotopic U251-luc or GBM09T-luc xenografts were injected with hypoxic exosomes secreted by GBM8401 cells with or without GPx1 knockdown at a dose of 20 μg exosome proteins once daily for one day on day 11 after tumor implantation. Then the mice were irradiated and followed for 3 consecutive days before tumor excision.

2.17. Animal irradiation and in vivo/in vitro clonogenic survival assay

Mice were locally irradiated (4.25 Gy/min) at a dose of 4 Gy under anesthesia using a high-energy X-ray linear accelerator (Varian). Tumors were then excised, minced, and dissociated for 30 min at 37 °C in Hanks' balanced salt solution containing 166 U/mL collagenase XI, 0.25 mg/mL protease, and 225 U/mL DNase. Cells were recovered by straining through an 80-μm mesh, centrifuging at 500 g, and resuspending in the culture medium. Cells were counted by hemocytometer using Trypan blue and assessed by *in vitro* clonogenic survival assay.

2.18. Immunofluorescence imaging

The mice tumor tissues were embedded in an OCT matrix (Shandon Lipshaw) and then frozen with liquid nitrogen. Frozen tissue sections (10 μm) were obtained using an OTF cryomicrotome (Bright-Hacker), fixed in ice-cold methanol for 10 min, and washed with PBS. To co-stain for pimonidazole and GPx1, the tumor sections were initially incubated with a FITC-conjugated anti-pimonidazole monoclonal antibody (1:250; Chemicon International) for 1 h at room temperature. The tumor sections were then co-stained for GPx1 using a monoclonal antibody (Thermo Fisher Scientific) at a final concentration of 10 μg/mL. The sections were washed three times in PBS, with each wash lasting 5 min. Next, the sections were incubated with DyLght 649-conjugated goat anti-rabbit antibody (1:100 dilution; Molecular Probes) and washed again for GPx1 staining. For human specimen staining studies, frozen sections of human glioblastoma were incubated with primary antibodies, GPx1 (1:200 dilution; Thermo Fisher Scientific) with or without HIF-1α (1:150 dilution; Novus Biologicals), overnight at 4 °C and secondary antibodies, DyLght 649-conjugated goat anti-rabbit antibody (1:100 dilution; Molecular Probes) or Dylight 488-conjugated goat anti-mouse antibody (1:100 dilution; Abcam). To stain for CD31/PECAM-1, the tumor sections were incubated with primary antibodies, CD31/PECAM-1(1:100 dilution; Novus Biologicals), overnight at 4 °C and secondary antibodies, DyLght 649-conjugated goat anti-rabbit antibody (1:100 dilution; Molecular Probes). TUNEL staining was carried out using the TUNEL Apoptosis Detection Kit (Millipore) according to the manufacturer's protocol. For CD31-TUNEL double staining, TUNEL staining was performed on slides pre-labeled with anti-CD31 antibody. At the end of the staining period, the sections were sealed with 90% glycerin in PBS containing an antifade medium DABCO (25 mg/mL) and DAPI (0.5 mg/mL). Tissue fluorescence was visualized using the Axio Observer A1 digital fluorescence microscope system (ZEISS). The nuclei staining was expressed as the percentage of TUNEL-positive apoptotic cells among 1000 cells in each tumor. The TUNEL-positive cells were counted in 40 high-power fields in 10 different sections for each tumor, 100 cells per section. The quantification of apoptotic endothelial cells (CD31/TUNEL) was measured as the average ratio of apoptotic endothelial cells to the total number of endothelial cells in 10 random fields using a 40× objective.

2.19. Bioluminescent imaging (BLI)

The engrafted tumors of mice were imaged using the IVIS Imaging System 200 Series (Calliper) to capture bioluminescent signals. To facilitate imaging, the mice were anesthetized with isoflurane and received an intraperitoneal injection of D-Luciferin (Calliper) at a dose of 250 μg/g body weight. Imaging was performed 15 min following the injection. To quantitatively analyze the BLI signal, regions of interest that encompassed the intracranial area of the signal were defined using Living Image, 2.60.1, and the total numbers of photons per second per steradian per square centimeter were recorded.

2.20. Bioinformatics analysis

The correlation between the expression of the GPx1 gene and the overall survival (OS) of glioma patients was evaluated using the dataset from Tumor Brain REMBRANDT study (Madhaven - 550 - MAS5.0 - u133p2) in the R2 Genomics Analysis and Visualization Platform (http://r2.amc.nl). Kaplan-Meier survival curves were generated using the optimal cutoff selected by the scan model. Additionally, the same dataset was utilized to investigate the GPx1 gene expression in different tumor grades and to assess the correlation of GPx1 with HIF-1α, HIF-1α target genes, and exosomal marker genes using the R2 web-based application.

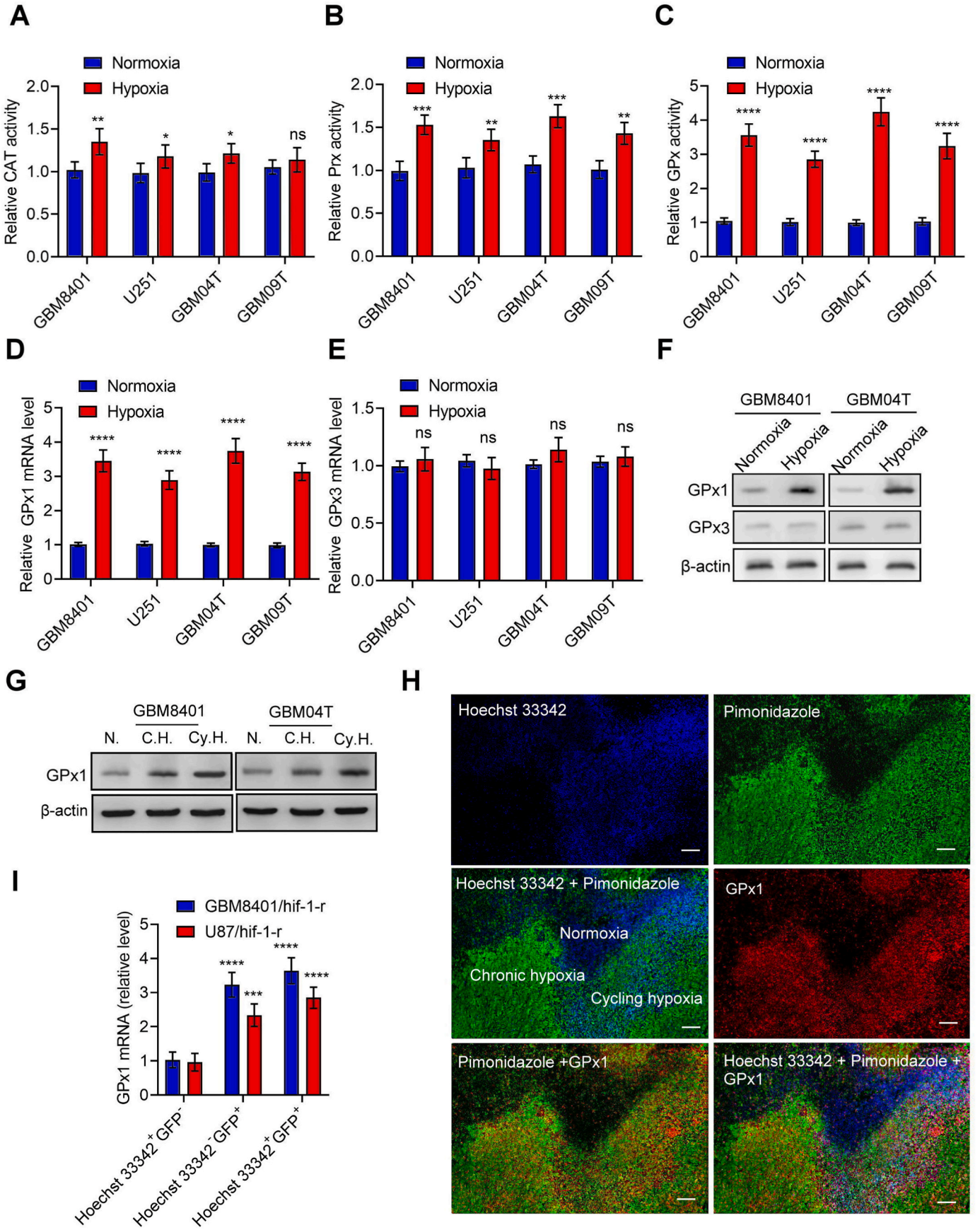

(caption on next page)

Fig. 1. Tumor hypoxia up-regulates GPx1 expression and function in glioblastoma.
(A–C) Enzyme activities of Catalase (CAT), peroxiredoxin (Prx), and glutathione peroxidase (GPx) in the human glioblastoma cells (GBM8401 and U251) and primary glioblastoma cells (GBM04T and GBM09T) at 24 h after normoxic and hypoxic treatment (<1% O_2). **(D–E)** mRNA levels of GPx1 or GPx3 in the GBM8401, U251, GBM04T, and GBM09T cells at 24 h after normoxic and hypoxic treatment (<1% O_2). **(F)** Protein levels of GPx1 or GPx3 in the GBM8401 and GBM04T cells at 24 h after normoxic and hypoxic treatment (<1% O_2). (**G**) Protein levels of GPx1 in the GBM8401 and GBM04T cells at 24 h after normoxia (N), non-interrupted (C.H.) hypoxia (<1% O_2), and cycling (Cy.H.) hypoxia (<1% O_2). (**H**) Immunostaining of GPx1 expression in hypoxic tumor subpopulations from GBM8401 xenografts. White color represents the colocalization of pimonidazole (green), Hoechst 33342 (blue), and GPx1 (red). (**I**) GPx1 mRNA levels in normoxic cells (Hoechst 33342^+ and GFP^-), chronic hypoxic cells (Hoechst 33342^- and GFP^+), and cycling hypoxic cells (Hoechst 33342^+ and GFP^+) isolated from disaggregated GBM8401/hif-1-r and U87/hif-1-r xenografts. Error bars, SD within triplicate experiments. *$p < 0.05$; **$p < 0.01$; ***$p < 0.001$; ****$p < 0.0001$, compared with normoxia. (For interpretation of the references to color in this figure legend, the reader is referred to the Web version of this article.)

2.21. Tissue arrays

The tissue arrays contained 6 cases of anaplastic oligodendroglioma, 26 cases of astrocytoma, 4 cases of glioblastoma multiforme, 17 cases of glioma, and 3 cases of normal brain tissues, with a single core per case; a total of 63 cases/63 cores (US Biomax, Inc.). Tissue arrays were analyzed by immunohistochemistry.

2.22. Immunohistochemistry (IHC)

IHC staining was carried out on glioma tissue arrays (Biomax) and tumor samples from 37 glioblastoma patients, utilizing the avidin-biotin-peroxidase complex method. The paraffin sections were deparaffinized and rehydrated with a graded series of ethanol (50%–100%). The endogenous peroxidase activity was blocked by treatment with 0.3% H_2O_2 for 15 min. The sections were then incubated with the primary antibody (1:100 dilution) overnight at 4 °C, followed by conjugation to the secondary antibody (1:100 dilution). Delafield's hematoxylin was used for counterstaining, after which the sections were dehydrated and mounted. Negative controls were stained without the primary antibodies. IHC staining was performed by two pathologists. The scoring criteria for GPx1 or HIF-1α immunostaining were based on clinical data, adopting the semiquantitative immunoreactive score (IRS) system. Category A (intensity of immunostaining) was scored using the following criteria: 0, negative; 1, weak; 2, moderate; and 3, strong. Category B (percentage of immunoreactive cells) was scored using the following criteria: 1 (0%–25%), 2 (26%–50%), 3 (51%–75%), and 4 (76%–100%). The GPx1 expressions were given scores ranging from 0 to 12 by multiplying the scores of categories A and B in the same section. The use of clinical samples was approved by the Institutional Review Board (CMUH110-REC3-030).

2.23. Statistical analysis

The data are expressed as mean ± SD. To analyze the differences between the experimental groups, one-way ANOVA followed by post hoc Scheffe test was performed using GraphPad Prism Software. The two-sided, unpaired Student's t-test was used to compare the control and experimental groups. Statistical significance was considered at $p < 0.05$.

3. Results

3.1. Tumor hypoxia up-regulates GPx1 expression and function in glioblastoma

To investigate the mechanism of H_2O_2 catabolism in glioblastoma cells under hypoxia, we first determined the enzyme activities of CAT, Prx, and GPx in the human primary glioblastoma cells (GBM04T and GBM09T) and human glioblastoma cells (GBM8901 and U251) with or without hypoxic stress (<1% O_2). The enzyme activities of CAT, Prx, and GPx in glioblastoma cells were upregulated after hypoxic treatment (Fig. 1A–C). However, the increased enzyme activities predominantly occurred in GPx, suggesting that GPx is the main enzyme for H_2O_2 catabolism in glioblastoma cells under hypoxia. GPx has eight different isoforms (GPx1–8) in *Homo sapiens* [7]. Among these isoforms, GPx1 and GPx3 are essential in scavenging H_2O_2. Therefore, we further analyzed the expression of GPx1 and GPx3 in glioblastoma cells under hypoxia. mRNA and protein levels of GPx1 and GPx3 were upregulated in the human glioblastoma cells after hypoxic treatment (Fig. 1D–F; S1A–S1C). However, there was no significant difference in GPx3 expression, indicating up-regulation of GPx1, but not GPx3 expression contributes to hypoxia-elevated GPx enzyme activity. In order to rule out the difference from room air oxygen condition (21%), we repeated the above experiments in physiological oxygen condition (12%). There is no significant difference between 21% and 12% oxygen conditions (Figs. S1D–S1I). Furthermore, glioblastoma cells present an upsurge of GPx1 in both mRNA and protein levels under chronic and cycling hypoxia (Fig. 1G; S1J and S1K). To authenticate the intra-glioblastoma GPx1 expression mediated by tumor hypoxia, we utilized immunofluorescence imaging concomitant with pimonidazole (a hypoxia marker) and Hoechst 33342 (a perfusion marker) to examine hypoxic tumor subpopulations from GBM8401 xenografts. A high degree of heterogeneity across the Hoechst 33342 and pimonidazole staining was present within the immunofluorescence imaging of GBM8401 xenografts (Fig. 1H). The GPx1 staining analysis demonstrated that the expression of GPx1 was detected in both chronic hypoxic (Hoechst 33342^- and pimonidazole$^+$) and cycling hypoxic (Hoechst 33342^+ and pimonidazole$^+$) areas of the tumors (Fig. S1L). We later conducted Q-PCR to analyze the GPx1 mRNA expression in the hypoxic cell subpopulations derived from disaggregated orthotopic U87/HIF1-r and GBM8401/HIF1-r xenografts [23]. The GPx1 mRNA expression increased substantially in the subpopulations of chronic and cycling hypoxia compared to normoxia (Fig. 1I). These findings revealed that tumor hypoxia elevates GPx1 expression and function in glioblastoma.

3.2. GPx1 is a HIF-1α target gene

In an effort to gain a deeper understanding of how hypoxia induces GPx1, we investigated the expression of GPx1 in glioblastoma cells by inhibiting HIF-1α or HIF-2α with genetic manipulation or chemicals under hypoxia. Notably, we found that the shRNA silencing of HIF-1α (but not HIF-2α) inhibited GPx1 protein levels induced by hypoxia (Fig. 2A–C; S2A and S2B). On the other hand, we observed the overexpression of HIF-1α in glioblastoma cells through the transfection of the deletion mutant plasmids of HIF1α-oxygen-dependent degradation domain (HIF-1-OD) significantly upregulated GPx1 protein levels under normoxia (Fig. 2D and E). Furthermore, the administration of HIF-1α inhibitor (LW6), but not HIF-2α inhibitor (PT2399), reduced hypoxia-induced transcriptional activation of GPx1 (Fig. 2F). Conversely, the co-expression of HIF-1-OD and GPx1-Luc plasmids exhibit an augmented reporter activity compared with the control group (Fig. 2G). Next, analysis using the Eukaryote promoter database identified a hypoxia-responsive element (HRE) site in the human GPx1 promoter sequence (−2000 ~ +1 bp; relative to transcription starting site) (Fig. 2H). In order to validate this binding motif, we introduced nucleotide alterations into this predicted HRE of pGPx1-Luc (Fig. 2I). Notably, the mutations of HRE on the GPx1 promoter negated the induction of GPx1 mediated by hypoxia. Moreover, ChIP assays followed by Q-PCR (ChIP-qPCR) revealed increased binding of HIF-1α to the HRE of GPx1 in glioblastoma cells compared with IgG (Fig. 2J and K). As a whole, these

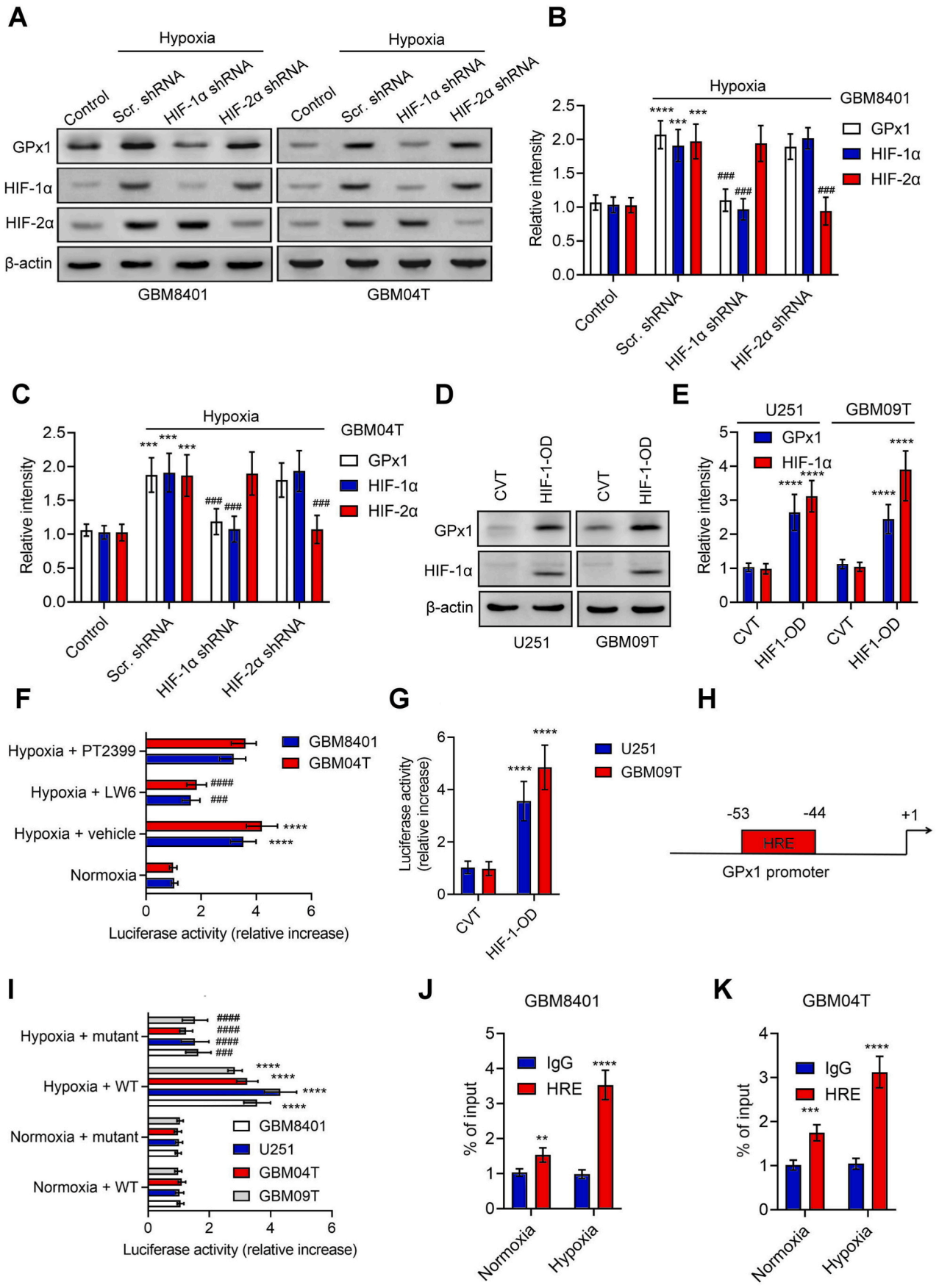

(caption on next page)

Fig. 2. GPx1 is a HIF-1α target gene. (**A, B,** and **C**) Protein levels of GPx1, HIF-1α, and HIF-2α in GBM8401 and GBM04T cells with or without HIF-1α or HIF-2α knockdown at 24 h after hypoxic treatment (<1% O_2). (**D** and **E**) Protein levels of GPx1 and HIF-1α in U251 and GBM09T cells transfected with the control (CVT) or HIF-1α-ODD deletion mutant plasmids (HIF1-OD) for 48 h. (**F**) Luciferase reporter activities of GPx1 promoter in GBM8401 and GBM04T cells with or without HIF-1α (LW6) or HIF-2α (PT2399) inhibitor at 24 h after hypoxic treatment (<1% O_2). (**G**) Luciferase reporter activities of GPx1 promoter in U251 and GBM09T cells co-transfected with HIF1-OD for 48 h. (**H**) One putative hypoxia response element (HRE) was identified in the human GPx1 promoter. (**I**) Luciferase activities of GBM8401, U251, GBM04T, and GBM09T cells that carry Renilla luciferase reporter plasmids cotransfected with the WT or mutant GPx1 promoter regions; the cells were treated with or without hypoxia (<1% O_2) for 24 h. (**J** and **K**) ChIP followed by real-time PCR (ChIP-qPCR) assay of HIF-1α binding in GPx1 promoter in response to hypoxia (<1% O_2) for 24 h; results are expressed as percentages of inputs. Error bars, SD within triplicate experiments. $^{**}p < 0.01$; $^{***}p < 0.001$; $^{****}p < 0.0001$, compared with control (normoxia), CVT, or IgG. $^{\#\#}p < 0.01$; $^{\#\#\#}p < 0.001$; $^{\#\#\#\#}p < 0.0001$, compared with hypoxia plus scramble (Scr.) shRNA groups or hypoxia plus vehicle groups.

findings suggest that tumor hypoxia regulates GPx1 by the direct binding of HIF-1α to GPx1's promoter.

3.3. GPx1 is a critical enzyme for H_2O_2 homeostasis and cell survival in glioblastoma cells under hypoxia

In light of GPx1's known role as an H_2O_2 scavenger, we sought to investigate whether hypoxia-mediated GPx1 upregulation plays a crucial role in preventing H_2O_2 overload and consequent cell death in glioblastoma cells under hypoxia. Using a lentiviral-based system, we knocked down GPx1 expression via two independent GPx1 target shRNAs, confirmed by Western blot analysis demonstrating significant decreases in GPx1 expression (Fig. 3A and Fig. S3A). We observed that the knockdown of GPx1 in GBM8401 and GBM04T cells substantially increased intracellular H_2O_2 levels (Fig. 3B and C), ROS levels (Fig. 3D and E, Fig. S3B and C), and reduced cell viabilities in hypoxia (Fig. 3F and Fig. S3D). Moreover, the loss of cell viability induced by GPx1 knockdown in hypoxia could be rescued by the apoptosis inhibitor, Z-VAD-FMK, but not by the necroptosis inhibitor, GSK872, or the ferroptosis inhibitor, ferrostatin-1 (Fig. 3G and Fig. S3E), indicating that apoptosis is the primary mode of cell death. Indeed, the percentages of apoptotic cells and caspase 3 activities were significantly increased in GPx1 knockdown cells following hypoxic treatment (Fig. 3H and I, Fig. S3F and G). Additionally, we stably transduced U251 and GBM09T cells with recombinant lentiviruses expressing GPx1 (Fig. 3J and Fig. S3H). Compared to control lentiviral vector-infected glioblastoma cells, GPx1-overexpressing glioblastoma cells exhibited resistance to H_2O_2-induced cell loss (Fig. 3K), decline in apoptosis (Fig. 3L), and decreased caspase 3 activities (Fig. 3M). Taken together, these findings suggest that GPx1 is a critical enzyme in preventing hypoxia-mediated H_2O_2 overload and apoptosis in glioblastoma cells.

3.4. Exosomal GPx1 promotes the resistance to H_2O_2 and radiation in glioblastoma and endothelial cells

Exosomes secreted by mesenchymal stem cells (MSCs) have been shown to contain GPx1 protein, which aids in the recovery of hepatic oxidant injury [30]. Exosomes secreted by hypoxic tumor cells also promote resistance to oxidative stress and radiation in normoxic tumor cells or other stromal cells [31]. Therefore, we postulated that GPx1 might play a role in the resistance to oxidative stress and radiation mediated by hypoxic exosomes. To test this hypothesis, we first isolated exosomes from glioblastoma cells with or without GPx1 knockdown under normoxic or hypoxic conditions and determined the levels of GPx1 protein in these exosomes. Increased GPx1 and exosomal markers, CD63 and CD81, were observed in hypoxic exosomes derived from control glioblastoma cells transfected with scramble shRNA (Fig. 4A and B). In comparison, GPx1, but not CD63 or CD81, decreased in hypoxic exosomes derived from glioblastoma cells after GPx1 knockdown. Moreover, hypoxic exosomes enhanced the resistance to H_2O_2 (Fig. 4C–F) or radiation (Fig. 4G and H, Fig. S4A) in glioblastoma and endothelial cells, which were reversed by GPx1 knockdown. This suggests that exosomal GPx1 induced by hypoxia contributes to the resistance to H_2O_2 or radiation in glioblastoma and endothelial cells. Additionally, we isolated exosomes secreted by glioblastoma cells with or without GPx1 overexpression. Compared with control lentiviral vector-infected glioblastoma cells, GPx1-overexpressing glioblastoma cells showed an increase in exosome-derived GPx1 (Figs. S4B and S4C). Exosomes secreted by GPx1-overexpressing glioblastoma cells increased the resistance to H_2O_2 or radiation in glioblastoma and endothelial cells compared to exosomes derived from control vector-expressing glioblastoma cells (Figs. S4D–S4J), indicating that exosomal GPx1 plays a protective role against H_2O_2 or radiation-induced apoptosis in glioblastoma and endothelial cells.

3.5. GPx1 is essential for glioblastoma growth and hypoxic exosomes-induced radiation resistance in vivo

To validate the biological impact of GPx1 *in vivo*, we employed Tet-regulatable lentiviral vectors encoding shRNAs to conditionally knockdown GPx1 upon doxycycline (Dox) in GBM04T-luc cells within the tumor microenvironment. The administration of Dox instigated inhibition of GPx1 expression (Fig. 5A and B), increased levels of ROS and H_2O_2 (Figs. S5A and S5B), reduced cell viability (Fig. 5C), augmented caspase 3 activities (Fig. 5D) and apoptosis (Fig. 5E) in primary glioblastoma cells under hypoxia. Following this, the cells were intracranially implanted into nude mice as orthotopic patient-derived glioblastoma (GBM04T) xenografts. The mice who received systemic delivery of Dox exhibited significant suppression of tumor growth (Fig. 5F and G) and promotion of apoptosis (Fig. 5H and I), indicating that GPx1 is vital for glioblastoma growth and survival within the tumor microenvironment. Furthermore, the Dox-induced knockdown of GPx1 was observed to substantially enhance the levels of H_2O_2 and protein carbamylation, an identifiable indicator of heightened oxidative stress [32], within the lysates of tumor tissue (Figs. S5C and S5D). These findings imply that the knockdown of GPx1 within the tumor microenvironment could potentially engender a notable surge in oxidative stress and subsequent induction of apoptosis. Subsequently, we investigated whether exosomal GPx1 plays an important role in tumor hypoxic exosome-mediated radiation resistance *in vivo*. Mice with orthotopic U251-luc xenografts were subjected to injection of hypoxic exosomes, secreted by GBM8401 cells with or without GPx1 knockdown, into the tumors once daily for 1 day; U251-luc xenografts were then irradiated and followed for 3 consecutive days before tumor excision. The injection of hypoxic exosomes substantially countered the irradiation-induced growth inhibition of U251-luc xenografts (Fig. 5J and K). In contrast, treating hypoxic exosomes with GPx1 depletion did not affect the growth of irradiated tumors. Histological examination confirmed that irradiation induced a decrease in microvessel density (Fig. 5L and Fig. S5E 5 M) and an increase in total apoptosis ($TUNEL^+$) (Fig. 5N) or endothelial cell apoptosis ($CD31^+TUNEL^+$) (Fig. 5O) in U251-luc xenografts. However, hypoxic exosomes-treated tumors significantly attenuated these effects, whereas hypoxic exosomes with GPx1 depletion-treated tumors restored the irradiation-induced vessel damage and apoptosis. Additionally, pretreatment with hypoxic exosomes, but not hypoxic exosomes with GPx1 depletion, significantly increased clonogenicity after radiation treatment in both U251 and GBM09T xenografts (Fig. 5P and Q). Hence, these results suggest that exosomal GPx1 plays a crucial role in tumor hypoxic exosome-mediated radiation resistance *in vivo*.

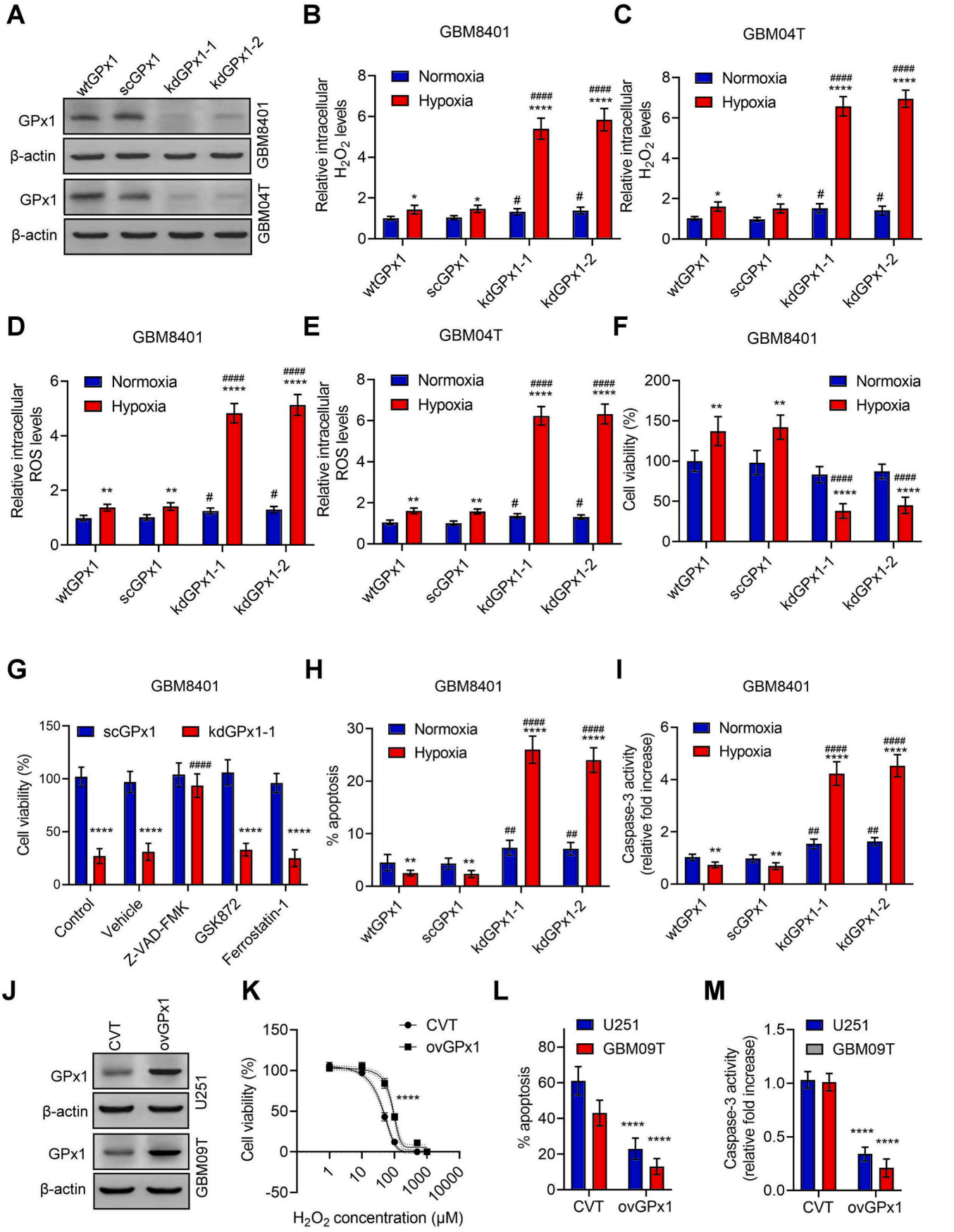

(caption on next page)

Fig. 3. GPx1 is a critical enzyme for H_2O_2 homeostasis and cell survival in glioblastoma cells under hypoxia. (**A**) Protein levels of GPx1 in wild-type GBM8401 or GBM04T cells (wtGPx1), control GBM8401 or GBM04T cells-expressing scramble shRNA (scGPx1), and GPx1 shRNAs (kdGPx1-1 or kdGPx-2) expressing GBM8401 or GBM04T. Relative intracellular H_2O_2 (**B** and **C**) and ROS (**D** and **E**) levels in glioblastoma cells cultured in normoxia or hypoxia (<1% O_2) with or without GPx1 knockdown for 24 h. Error bars, SD within triplicate experiments. *$p < 0.05$; ****$p < 0.0001$, compared with nomoxia. $^{\#}p < 0.05$; $^{\#\#\#\#}p < 0.0001$, compared with scGPx1. (**F**) Cell viabilities in GBM8401 cells cultured in normoxia or hypoxia (<1% O_2) with or without GPx1 knockdown for 48 h. Error bars, SD within triplicate experiments. **$p < 0.01$; ****$p < 0.0001$, compared with nomoxia. $^{\#\#\#\#}p < 0.0001$, compared with scGPx1. (**G**) Cell viabilities in GBM8401 cells with or without GPx1 knockdown pretreated with apoptosis inhibitor (Z-VAD-FMK, 60 μM), necroptosis inhibitor (GSK872, 5 μM), or ferroptosis inhibitor (ferrostatin-1, 1 μM) and cultured in hypoxia (<1% O_2) for 48 h. Error bars, SD within triplicate experiments. ****$p < 0.0001$, compared with scGPx1. $^{\#\#\#\#}p < 0.0001$, compared with vehicle. Percentages of apoptotic cells (**H**) and caspase-3 activities (**I**) in GBM8401 cells cultured in normoxia or hypoxia (<1% O_2) with or without GPx1 knockdown for 48 h. Error bars, SD within triplicate experiments. **$p < 0.01$; ****$p < 0.0001$, compared with nomoxia. $^{\#\#\#\#}p < 0.0001$, compared with scGPx1. (**J**) Protein levels of GPx1 in U251 and GBM09T cells lentivirally transduced with control vector (CVT) or GPx1-overexpressing vector (ovGPx1) for 3 days. (**K**) Dose-response curves representing the cell viability percentages (%) of glioblastoma cells with or without GPx1 overexpression treated with different concentrations of H_2O_2 for 48 h ****$p < 0.0001$, compared with CVT. Percentages of apoptotic cells (**L**) and caspase-3 activities (**M**) in glioblastoma cells with or without GPx1 overexpression treated with H_2O_2 (50 μM) for 48 h. Error bars, SD within triplicate experiments. ****$p < 0.0001$, compared with CVT.

3.6. GPx1 expression in glioblastoma patients is associated with HIF-1α expression, poor outcomes, the expression of HIF-1α target genes, and exosome markers

To determine the clinical relevance of GPx1 expression in glioblastoma, we conducted immunohistochemical (IHC) studies on human glioblastoma specimens. Significantly higher GPx1 expression was present in glioblastoma compared to matched normal tissues (Fig. 6A). Additionally, glioma tissue arrays containing 63 glioma samples demonstrated higher expressions and scores of GPx1 in high-grade glioma than in low-grade glioma or normal brain tissues (Fig. 6B–D). Further IHC studies on 32 glioblastoma samples showed a positive correlation between high levels of GPx1 gene expression and poor survival rates (Fig. 6E), thereby indicating the association of high GPx1 expression with unfavorable clinical outcomes in glioblastoma. Immunofluorescence imaging studies also showed a co-localization of GPx1 expression with HIF-1α in glioblastoma specimens (Fig. 6F and Fig. S6A). Another study involving 12 human glioblastoma samples showed a linear correlation between GPx1 and HIF-1α expression (Fig. 6G). Furthermore, GPx1 protein was found to be expressed much higher in exosomes than in cells for two human glioblastoma specimens (Fig. S6B). In addition, the analysis of a publicly available gene expression dataset (REMBRANDT) [33] revealed that GPx1 expression was correlated with poor outcomes (Fig. 6H), tumor grades (Fig. 6I), and positively associated with HIF-1α (Fig. 6J) but not EPAS1 (HIF-2α) (Fig. 6K). Furthermore, GPx1 expression was found to be linked to HIF-1α target genes such as HK2 (Fig. 6L), LDHA (Fig. 6M), VEGFA (Fig. S6C), and ENO1 (Fig. S6D), as well as exosomal marker genes such as CD63 (Fig. 6N), CD81 (Fig. 6O), and CD9 (Fig. S6E) in patients with glioma. These findings provide evidence for the clinical relevance of hypoxia or HIF-1α-regulated GPx1 expression in glioblastoma and support the role of exosome-mediated GPx1 delivery in human glioblastoma.

4. Discussion

The results of our prior studies revealed that tumor hypoxia elicits an upsurge in ROS levels in tumor cells by inducing NOX4 expression, which in turn promotes malignant progression, growth, and radioresistance in glioblastoma [34–36]. Similar results have been observed in other cancer types [37–40]. Regarding the liaison between NOX4 and tumorigenesis, H_2O_2 is considered to be an indispensable component not only because it serves as one of the major products of NOX4 but also its role as a second messenger regulating numerous interconnected signaling pathways [41]. Despite the generation of excess H_2O_2 induced by tumor hypoxia, tumor cells seem to acquire a mechanism for the metabolism of H_2O_2 to prevent excessive cytotoxicity resulting from ROS accumulation [42]. However, the intricacies of this mechanism are currently unknown. Our findings demonstrate that in glioblastoma cells, hypoxia-induced changes in enzyme activity were more significant for GPx than for CAT and Prx, suggesting that GPx are the primary enzymes for H_2O_2 catabolism under tumor hypoxia. Moreover, tumor hypoxia induced GPx1 but not GPx3 expression in glioblastoma cells. GPx1 knockdown resulted in H_2O_2 overload and apoptosis *in vitro*, as well as growth inhibition *in vivo*. Our *in vivo* results also indicate that both cycling and chronic hypoxic areas are involved in the tumor microenvironment-mediated induction of GPx1 in glioblastoma xenografts. Furthermore, expression of GPx1 increased significantly in isolated cycling and chronic hypoxic cells compared with isolated normoxic cells. These findings suggest that GPx1 controls the negative feedback of preventing excessive H_2O_2 and ensuing cell death under hypoxia. Further research is necessary to examine whether similar impacts and mechanisms occur in other tumor cells.

It has been shown that the transcription of human GPx1 is regulated by oxygen tension with the two oxygen response elements (OREs) in its promoter [43]. Decreased oxygen tension in cardiomyocytes during hypoxia has been found to decrease GPx1 expression by reducing the Ku protein association with the OREs [44]. However, whether the same phenotype exists in tumor cells has been subject to debate [45]. As to how the expression of GPx1 is regulated in tumors under hypoxic stress, we present here, for the first time, that HIF-1α directly binds to the HRE motif in the GPx1 promoter and further increases its transactivation in hypoxic glioblastoma cells. Colocalization of GPx1 expression with high expression of HIF-1α in human glioblastoma specimens and GPx1's positive association with HIF-1α and its target gene expression further supports this notion. These data are consistent with previous studies showing that HIF-1α regulates GPx1 expression in response to TGF-β1 treatment in colon cancer cells [46]. Our results corroborate that GPx1 is indeed a target gene of HIF-1α.

Several pieces of evidence suggest that GPx1 plays a pivotal role in tumor progression and resistance to therapy for glioblastoma. Firstly, unlike catalase and SOD, the expression of GPx1 in glioblastoma cells is diverse and heterogeneous in the tumor microenvironment. GPx1-expressing glioblastoma cells are highly sensitive to oxidative stress after the inhibition of GPx1, indicating the pivotal role of GPx1 in regulating oxidative stress in glioblastoma cells [47]. Secondly, the knockdown of GPx1 in glioblastoma cells impairs tumor growth and invasion while also inducing apoptosis *in vitro*. GPx1 is also a downstream target gene for non-POU domain-containing octamer-binding protein (NONO)-mediated mRNA splicing, making it a crucial factor in the NONO-promoted glioblastoma progression [48]. Thirdly, glioma stem cells (GSCs) exhibit high expression of GPx1, which contributes to radioresistance and stemness of GSCs [49]. Fourthly, proteomic analysis of mitochondria isolated from primary human glioblastoma and peritumoral tissues demonstrated upregulated GPx1 expression in glioblastoma tissues [50]. Our results indicate that GPx1 is a critical enzyme in preventing H_2O_2 overload-induced cytotoxicity in glioblastoma under *in vitro* hypoxia or *in vivo* tumor microenvironments. Even though excess H_2O_2 can induce various forms of cell death, such as apoptosis, necroptosis, or ferroptosis [51,52], our results showed that apoptosis is the primary cell death pathway in GPx1 depletion-induced cytotoxicity for glioblastoma cells in hypoxia. Collectively, these findings provide the

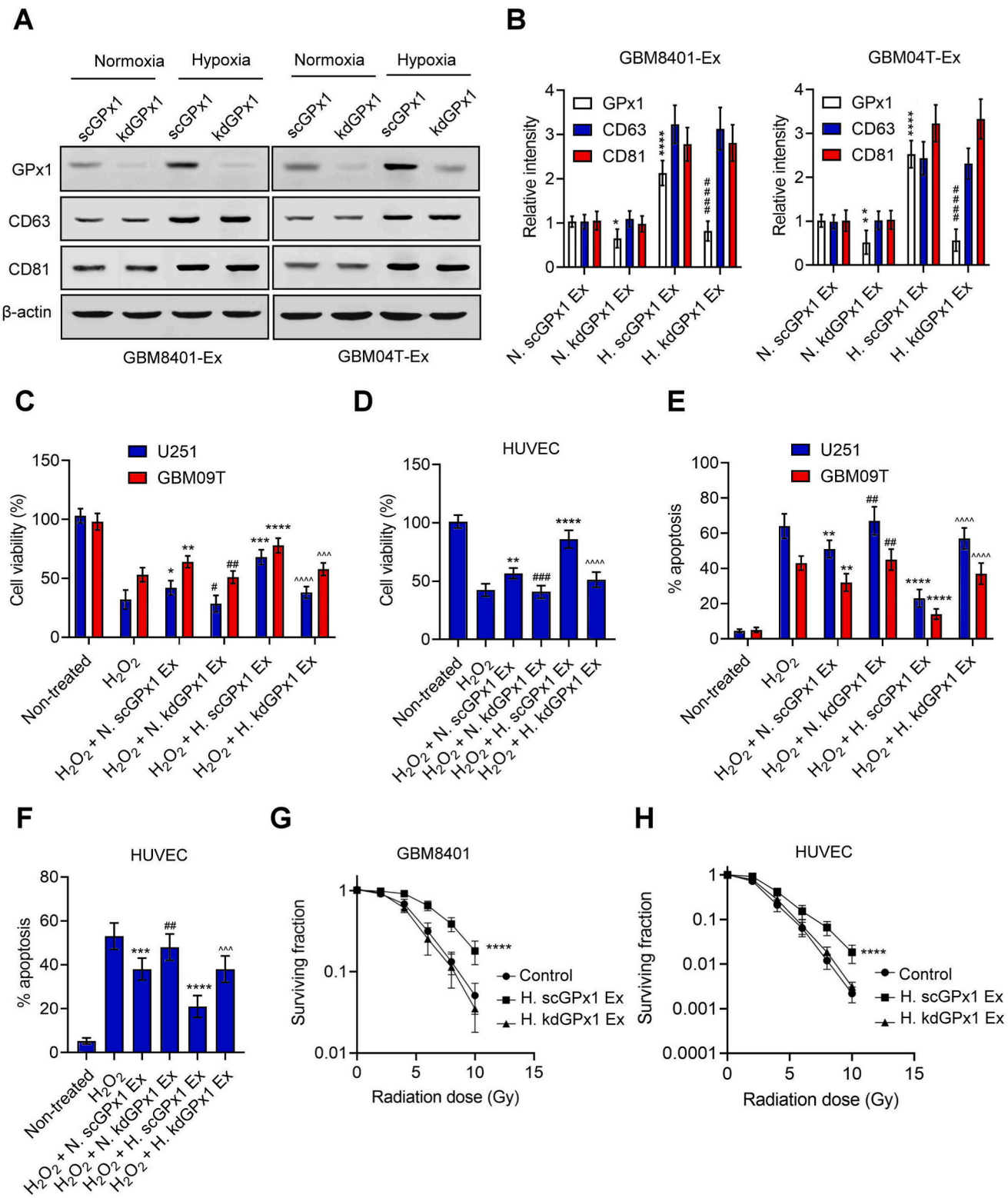

Fig. 4. Exosomal GPx1 promotes the resistance to H_2O_2 and radiation in glioblastoma and endothelial cells (**A** and **B**) Western blot analyses of GPx1, CD63, and CD81 levels in normoxic or hypoxic exosomes derived from GBM8401 or GBM04T cells expressing scramble shRNA (scGPx1) or GPx1 shRNAs (kdGPx1). N. scGPx1 Ex and N. kdGPx1 Ex are the normoxic exosomes derived from glioblastoma cells with or without GPx1 knockdown under normoxia. H. scGPx1 Ex and H. kdGPx1 Ex represent hypoxic exosomes secreted by glioblastoma cells with or without GPx1 knockdown under hypoxia (<1% O_2). Error bars, SD within triplicate experiments. *$p < 0.05$; **$p < 0.01$, ****$p < 0.0001$, compared with normoxic exosomes derived from control glioblastoma cells expressing scramble shRNA (N. scGPx1 Ex). $^{\#\#\#\#}p < 0.0001$, compared with hypoxic exosomes derived from control glioblastoma cells expressing scramble shRNA (H. scGPx1 Ex). Cell viabilities (**C** and **D**) and percentages of apoptotic cells (**E** and **F**) in glioblastoma cells (U251 and GBM09T) and endothelial cells (HUVEC) pretreated with normoxic or hypoxic exosomes, then subjected to H_2O_2 (50 μM) for 48 h. (**G** and **H**) Radiation cell survival fractions for GBM8401 and HUVEC cells pretreated with hypoxic exosomes, then subjected to radiation. Error bars, SD within triplicate experiments. *$p < 0.05$; **$p < 0.01$, ***$p < 0.001$, ****$p < 0.0001$, compared with H_2O_2 groups. $^{\#}p < 0.05$; $^{\#\#}p < 0.01$; $^{\#\#\#}p < 0.001$, compared with H_2O_2 + N. scGPx1 Ex groups; $^{\wedge\wedge\wedge}$ $p < 0.001$, $^{\wedge\wedge\wedge\wedge}$ $p < 0.0001$, compared with H_2O_2 + H. scGPx1 Ex groups.

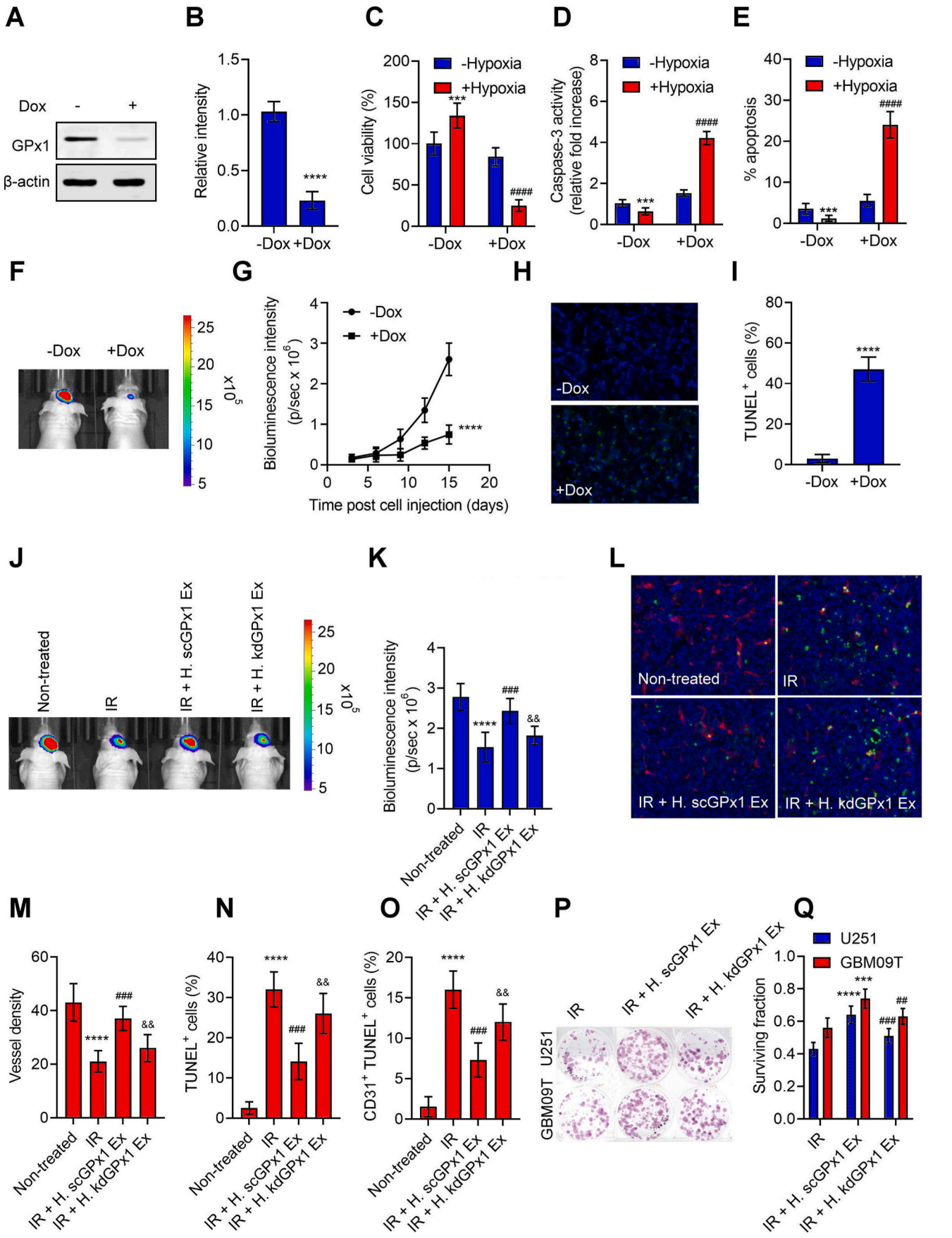

(caption on next page)

Fig. 5. GPx1 is essential for glioblastoma growth and hypoxic exosome-induced radiation resistance *in vivo*. (**A** and **B**) Western blot analyses of GPx1 expression in GBM04T-lucGFP cells with or without GPx1 knockdown by Tet-regulatable lentiviral knockdown system. The lentiviral-infected cells were treated for 48 h with Dox (0.04 μg/mL) to induce GPx1 knockdown. Error bars, SD within triplicate experiments. ****$p < 0.0001$, compared with no Dox treatment (−Dox). Cell viabilities (**C**), caspase-3 activities (**D**), and percentages of apoptotic cells (**E**) in glioblastoma cells cultured in normoxia or hypoxia (<1% O_2) with or without GPx1 knockdown for 48 h. Cells were pretreated for 48 h with Dox (0.04 μg/mL) to induce GPx1 knockdown and exposed to hypoxic stress. Error bars, SD within triplicate experiments. ***$p < 0.001$, ****$p < 0.0001$, compared with no Dox treatment under normoxia. $^{\#\#\#\#}p < 0.0001$, compared with no Dox treatment under hypoxia. (**F–I**) Represents the same group: GBM04T-lucGFP xenografts with or without Dox-induced GPx1 knockdown on day 15 after tumor implantation (**F**) Bioluminescent images for each group. (**G**) Mean bioluminescent intensity values associated with longitudinal monitoring of intracranial tumor growth for each group. Data are presented as means ± SD ($n = 6$). ****$p < 0.0001$ compared to no Dox treatment (−Dox). (**H**) TUNEL staining of tumor slices for each group. Apoptotic cells were stained by TUNEL (green). The nucleus was stained with DAPI (blue). (**I**) Percentages of apoptotic cells on each cross-section. ****$p < 0.0001$ compared to no Dox treatment (−Dox). (**J–O**) Represents the same group: U251-luc xenografts subjected to nothing (non-treated), radiation treatment (IR), pretreatment of hypoxic and GPx1 scramble knockdown exosomes excreted by GBM8401 plus radiation treatment (IR + H. scGPx1 Ex), and pretreatment of hypoxic and GPx1 depletion exosomes excreted by GBM8401 plus radiation treatment (IR + H. kdGPx1 Ex). Radiation was treated on day 20 after tumor implantation. (**J**) Bioluminescent images for each group. (**K**) Mean bioluminescent intensity values for each group. Data are presented as means ± SD ($n = 6$). ****$p < 0.0001$ compared to non-treated groups. $^{\#\#\#}p < 0.001$ compared to IR groups. $^{\&\&}p < 0.01$ compared to IR plus H. scGPx1 Ex groups. (**L**) Representative images of DAPI (blue), CD31 (red), and TUNEL (green) staining of tumor slices for each group. Quantifications of microvessel density (**M**), total apoptotic density (**N**), and endothelial cell apoptosis density (**O**) for each group. ***$p < 0.0001$ compared to non-treated groups. $^{\#\#\#}p < 0.001$ compared to IR groups. $^{\&\&}p < 0.01$ compared to IR plus H. scGPx1 Ex groups. Colony images (**P**) and surviving fractions (**Q**) in excised U251 and GBM09T xenografts after radiation treatment (IR), pretreatment of hypoxic and GPx1 scramble knockdown exosomes excreted by GBM8401 plus radiation treatment (IR + H. scGPx1 Ex), and pretreatment of hypoxic and GPx1 depletion exosomes excreted by GBM8401 plus radiation treatment (IR + H. kdGPx1 Ex). Radiation was treated on day 20 after tumor implantation. Error bars, SD within triplicate experiments. ***$p < 0.001$; ***$p < 0.0001$ compared to IR groups. $^{\#\#}p < 0.01$; $^{\#\#\#}p < 0.001$, IR + H. scGPx1 Ex groups. (For interpretation of the references to color in this figure legend, the reader is referred to the Web version of this article.)

rationale for targeting GPx1 as a novel therapeutic strategy in glioblastoma.

H_2O_2 possesses the ability to diffuse from tumor cells towards adjoining vascular endothelial cells and regulate intracellular signaling involved in cell growth or death [53]. However, this raises a captivating query: why does the elevated concentration of H_2O_2 within the tumor not result in the demise of vascular endothelial cells or hinder tumor angiogenesis? In addition, the vascular endothelial cells present within the tumor exhibit resistance towards radiation, which consequently impacts the effectiveness of radiation therapy for tumors [54–56]. Prior research has demonstrated that H_2O_2, radiation, or tumor hypoxia can stimulate the angiogenic factor, Vascular endothelial growth factor (VEGF), and these VEGF molecules can further insulate vascular endothelial cells against oxidative stress or radiation-induced injuries [57–59]. As a result, anti-VEGF inhibitors, or a combination of such inhibitors and radiation therapy, are employed to suppress angiogenesis and expedite the demise of tumor vascular endothelial cells [60]. However, these therapies have proven futile in glioblastoma or other cancers [61,62], which indicates that tumor vascular endothelial cells are impervious to oxidative stress or radiation damage and may employ other mechanisms that are as yet unknown. In this study, we discovered a new mechanism whereby hypoxic tumor cells increase exosomal GPx1 secretion. These exosomal GPx1 enzymes instigate resistance in vascular endothelial cells against apoptosis induced by oxidative stress or radiation. Hence, GPx1 inhibitors could suppress this mechanism and resensitize tumor vessels to oxidative stress or radiation damage.

Exosomes hold pivotal roles in the immunosuppressive, metastatic, and treatment-resistant pathways of multiple cancer types, including glioblastoma [63]. Various studies have revealed a significant correlation between hypoxia-triggered exosomes and glioblastoma progression. Tumor hypoxia propels the exosomal miR-301a secretion by glioblastoma cells, which triggers Wnt/β-catenin and reduces radiation sensitivity by targeting the tumor suppressor gene, TCEAL7 [64]. Additionally, VEGF-A expression is augmented in hypoxic glioblastoma-derived exosomes, which boosts the permeability of the blood-brain barrier by disrupting the expression of claudin-5 and occludin [65]. Many contents have been detected in tumor-derived exosomes, including proteins and miRNAs, but none have suggested the presence of antioxidant-related proteins in tumor-derived exosomes. Notably, a previous study revealed that exosomes derived from human mesenchymal stem cells contained GPx1, and these exosomal GPx1 demonstrated the ability to restore liver injury caused by oxidative stress [30]. In this study, we provide the first evidence that tumor-derived exosomes contain GPx1 protein, and hypoxia intensifies the exosomal GPx1 expression. These exosomal GPx1 play a crucial role in the resistance to H_2O_2 or radiation-induced apoptosis in glioblastoma and endothelial cells *in vitro* and *in vivo*. These findings support the notion that GPX1 in hypoxic tumor cells influences adjacent normoxic tumor and stromal cells, subsequently mitigating the sensitivity of these cells to oxidative stress or radiation.

The bioinformatics analysis of the Cancer Genome Atlas (TCGA) public database has revealed that GPx1 exhibits higher expression levels in glioma tissues compared to adjacent normal controls, and its expression is associated with poor survival outcomes [66]. In accordance with these findings, our bioinformatics analysis of another glioma dataset (REMBRANDT) [33] also demonstrated that GPx1 expression correlates with poor outcomes and tumor grades. Furthermore, GPx1 expression positively correlates with the expression of HIF-1α, HIF-1α target genes, and exosomal marker genes. While mRNA expression does not always predict protein abundance or enzyme activity, our immunohistochemical and immunofluorescence analyses further corroborate that GPx1 expression correlates with poor outcomes, tumor grade, and HIF-1α expression in glioblastoma patients. Additionally, we detected GPx1 protein in cells and exosomes derived from human glioblastoma specimens. These findings underline the clinical relevance of HIF-1α-regulated GPx1 and tumor exosomal GPx1 expression.

In conclusion, this study presents the first report that tumor hypoxia prevents H_2O_2 overload-induced cytotoxicity by activating GPx1 expression with HIF-1α in glioblastoma. Furthermore, our results provide evidence that hypoxic tumor-derived exosomes contain high levels of GPx1 and that exosomal GPx1 plays a critical role in providing resistance to oxidative stress and radiation for both tumor and endothelial cells *in vitro* and *in vivo*. These observations suggest that GPx1 could hold significant potential as a therapeutic target in suppressing glioblastoma.

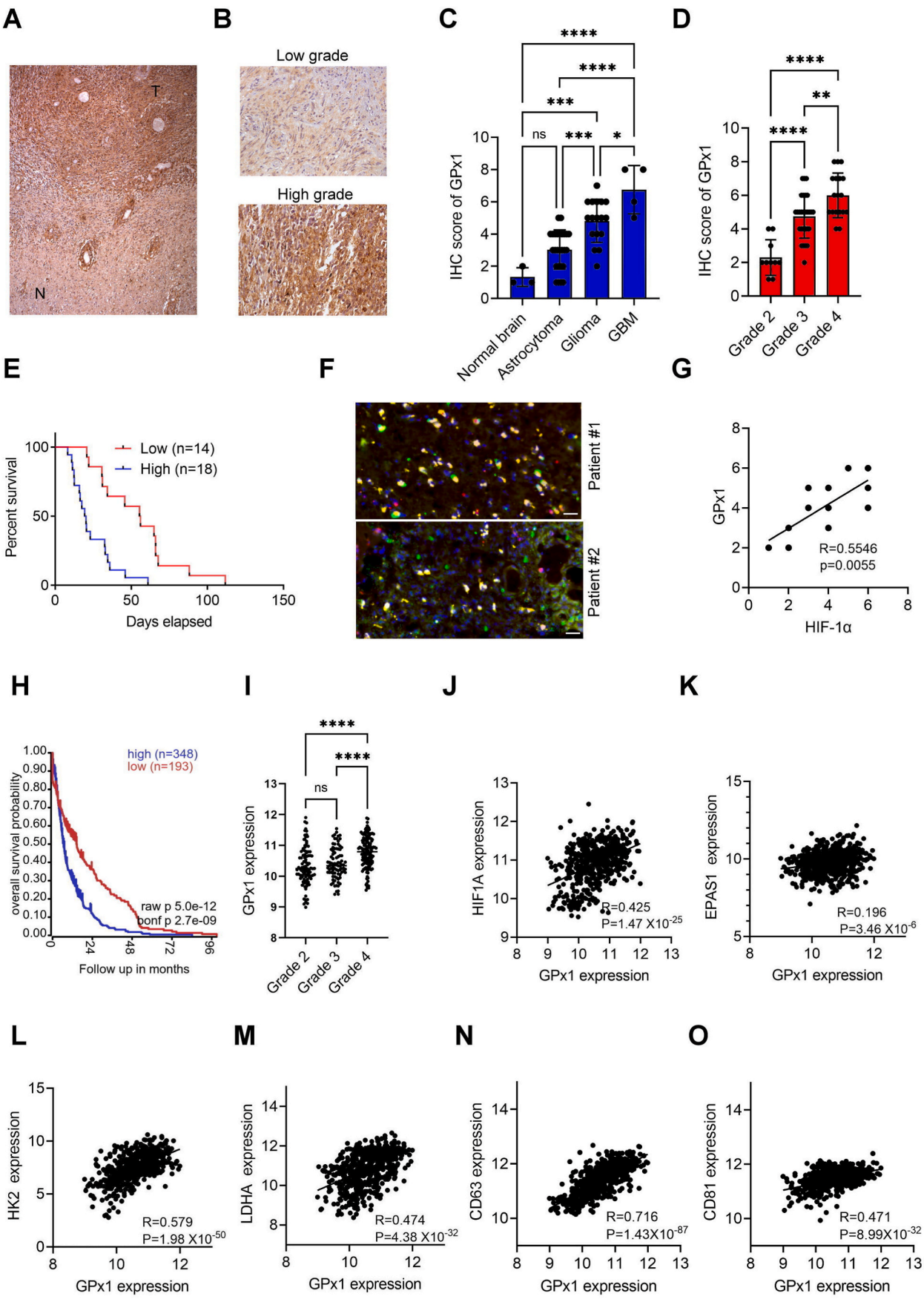

(caption on next page)

Fig. 6. GPx1 expression in glioblastoma patients is associated with HIF-1α expression, poor outcomes, the expression of HIF-1α target genes, and exosome markers. (**A** and **B**) Immunohistochemical staining of GPx1 in human low-grade and high-grade glioma samples. T means tumor whereas N represents normal brain tissues. (**C** and **D**) Immunohistochemical scores of GPx1 expression in brain glioma tissue arrays. (**E**) Kaplan-Meier analyses of the overall survival rate of 32 glioblastoma patients relative to GPx1 expression. GPx1 expression in glioblastoma samples was determined by immunohistochemical staining. (**F**) Immunofluorescence imaging of GPx1 and HIF-1α expression in human glioblastoma specimens. (**G**) Gene associations between GPx1 and HIF-1α in 12 human glioblastoma samples. (**H**) Survival curves comparing patients with high (blue) and low (red) GPx1 expression in glioma using the REMBRANDT dataset. (**I**) Box plots comparing GPx1 expression in various grades of glioma using the REMBRANDT dataset. (**J**–**O**) Gene correlation of GPx1/HIF1A, GPx1/EPAS1, GPx1/HK2, GPx1/LDHA, GPx1/CD63 or GPx1/CD81 in glioma using the REMBRANDT dataset. Error bars, SD within triplicate experiments. *p < 0.05, **p < 0.01, ***p < 0.001, ****p < 0.0001 compared to corresponding groups. (For interpretation of the references to color in this figure legend, the reader is referred to the Web version of this article.)

Declaration of competing interest

The authors have declared no potential conflict of interest.

Data availability

Data will be made available on request.

Acknowledgments

Grant support was provided by the Ministry of Science and Technology of the Republic of China (Grant Nos. NSTC 110-2628-B-039-006, NSTC 111-2314-B-039-032 and NSTC 111-2314-B-906-002) and the China Medical University and Hospital (Grant Nos. DMR-112-133, DMR-112-079, CMU111-MF-99, CMU109-AWARD-01), the China Medical University Hsinchu Hospital (CMUHCH-DMR-111-007) and China Medical University An Nan Hospital (ANHRF111-53).

Appendix A. Supplementary data

Supplementary data to this article can be found online at https://doi.org/10.1016/j.redox.2023.102831.

References

[1] C. Lennicke, J. Rahn, R. Lichtenfels, L.A. Wessjohann, B. Seliger, Hydrogen peroxide - production, fate and role in redox signaling of tumor cells, Cell Commun. Signal. 13 (2015) 39.
[2] H. Sies, Role of metabolic H2O2 generation: redox signaling and oxidative stress, J. Biol. Chem. 289 (2014) 8735–8741.
[3] H. Sies, Hydrogen peroxide as a central redox signaling molecule in physiological oxidative stress: oxidative eustress, Redox Biol. 11 (2017) 613–619.
[4] J.R. Stone, S. Yang, Hydrogen peroxide: a signaling messenger, Antioxidants Redox Signal. 8 (2006) 243–270.
[5] M. Alfonso-Prieto, X. Biarnes, P. Vidossich, C. Rovira, The molecular mechanism of the catalase reaction, J. Am. Chem. Soc. 131 (2009) 11751–11761.
[6] S.G. Rhee, Overview on peroxiredoxin, Mol. Cell. 39 (2016) 1–5.
[7] R. Brigelius-Flohe, M. Maiorino, Glutathione peroxidases, Biochim. Biophys. Acta 1830 (2013) 3289–3303.
[8] F. Weinberg, N. Ramnath, D. Nagrath, Reactive oxygen species in the tumor microenvironment: an overview, Cancers (Basel) 11 (2019).
[9] S. Rodic, M.D. Vincent, Reactive oxygen species (ROS) are a key determinant of cancer's metabolic phenotype, Int. J. Cancer 142 (2018) 440–448.
[10] G. Pani, B. Bedogni, R. Colavitti, R. Anzevino, S. Borrello, T. Galeotti, Cell compartmentalization in redox signaling, IUBMB Life 52 (2001) 7–16.
[11] N.S. Chandel, D.S. McClintock, C.E. Feliciano, T.M. Wood, J.A. Melendez, A. M. Rodriguez, P.T. Schumacker, Reactive oxygen species generated at mitochondrial complex III stabilize hypoxia-inducible factor-1alpha during hypoxia: a mechanism of O2 sensing, J. Biol. Chem. 275 (2000) 25130–25138.
[12] N.S. Chandel, E. Maltepe, E. Goldwasser, C.E. Mathieu, M.C. Simon, P. T. Schumacker, Mitochondrial reactive oxygen species trigger hypoxia-induced transcription, Proc. Natl. Acad. Sci. U.S.A. 95 (1998) 11715–11720.
[13] J.J. Lum, T. Bui, M. Gruber, J.D. Gordan, R.J. DeBerardinis, K.L. Covello, M. C. Simon, et al., The transcription factor HIF-1alpha plays a critical role in the growth factor-dependent regulation of both aerobic and anaerobic glycolysis, Genes Dev. 21 (2007) 1037–1049.
[14] F. Paredes, H.C. Williams, A. San Martin, Metabolic adaptation in hypoxia and cancer, Cancer Lett. 502 (2021) 133–142.
[15] I. Diebold, A. Petry, J. Hess, A. Gorlach, The NADPH oxidase subunit NOX4 is a new target gene of the hypoxia-inducible factor-1, Mol. Biol. Cell 21 (2010) 2087–2096.
[16] H. Awad, N. Nolette, M. Hinton, S. Dakshinamurti, AMPK and FoxO1 regulate catalase expression in hypoxic pulmonary arterial smooth muscle, Pediatr. Pulmonol. 49 (2014) 885–897.
[17] Q.S. Wang, Y.M. Zheng, L. Dong, Y.S. Ho, Z. Guo, Y.X. Wang, Role of mitochondrial reactive oxygen species in hypoxia-dependent increase in intracellular calcium in pulmonary artery myocytes, Free Radic. Biol. Med. 42 (2007) 642–653.
[18] H.J. Kim, H.Z. Chae, Y.J. Kim, Y.H. Kim, T.S. Hwangs, E.M. Park, Y.M. Park, Preferential elevation of Prx I and Trx expression in lung cancer cells following hypoxia and in human lung cancer tissues, Cell Biol. Toxicol. 19 (2003) 285–298.
[19] L. Nonn, M. Berggren, G. Powis, Increased expression of mitochondrial peroxiredoxin-3 (thioredoxin peroxidase-2) protects cancer cells against hypoxia and drug-induced hydrogen peroxide-dependent apoptosis, Mol. Cancer Res. 1 (2003) 682–689.
[20] Y.J. Kim, J.Y. Ahn, P. Liang, C. Ip, Y. Zhang, Y.M. Park, Human prx1 gene is a target of Nrf2 and is up-regulated by hypoxia/reoxygenation: implication to tumor biology, Cancer Res. 67 (2007) 546–554.
[21] M. Zhang, M. Hou, L. Ge, C. Miao, J. Zhang, X. Jing, N. Shi, et al., Induction of peroxiredoxin 1 by hypoxia regulates heme oxygenase-1 via NF-kappaB in oral cancer, PLoS One 9 (2014), e105994.
[22] S.T. Wei, J.Y. Chiang, H.L. Wang, F.J. Lei, Y.C. Huang, C.C. Wang, D.Y. Cho, et al., Hypoxia-induced CXC chemokine ligand 14 expression drives protumorigenic effects through activation of insulin-like growth factor-1 receptor signaling in glioblastoma, Cancer Sci. 114 (2023) 174–186.
[23] C.W. Chou, C.C. Wang, C.P. Wu, Y.J. Lin, Y.C. Lee, Y.W. Cheng, C.H. Hsieh, Tumor cycling hypoxia induces chemoresistance in glioblastoma multiforme by upregulating the expression and function of ABCB1, Neuro Oncol. 14 (2012) 1227–1238.
[24] C.H. Hsieh, J.W. Kuo, Y.J. Lee, C.W. Chang, J.G. Gelovani, R.S. Liu, Construction of mutant TKGFP for real-time imaging of temporal dynamics of HIF-1 signal transduction activity mediated by hypoxia and reoxygenation in tumors in living mice, J. Nucl. Med. 50 (2009) 2049–2057.
[25] K.J. Nelson, D. Parsonage, Measurement of peroxiredoxin activity, Curr Protoc Toxicol (2011). Chapter 7:Unit7 10.
[26] S.T. Wei, Y.C. Huang, J.Y. Chiang, C.C. Lin, Y.J. Lin, W.C. Shyu, H.C. Chen, et al., Gain of CXCR7 function with mesenchymal stem cell therapy ameliorates experimental arthritis via enhancing tissue regeneration and immunomodulation, Stem Cell Res. Ther. 12 (2021) 314.
[27] C.H. Hsieh, C.H. Lee, J.A. Liang, C.Y. Yu, W.C. Shyu, Cycling hypoxia increases U87 glioma cell radioresistance via ROS induced higher and long-term HIF-1 signal transduction activity, Oncol. Rep. 24 (2010) 1629–1636.
[28] C.H. Hsieh, Y.J. Lin, C.P. Wu, H.T. Lee, W.C. Shyu, C.C. Wang, Livin contributes to tumor hypoxia-induced resistance to cytotoxic therapies in glioblastoma multiforme, Clin. Cancer Res. 21 (2015) 460–470.
[29] B.L. Carlson, J.L. Pokorny, M.A. Schroeder, J.N. Sarkaria, Establishment, maintenance and in vitro and in vivo applications of primary human glioblastoma multiforme (GBM) xenograft models for translational biology studies and drug discovery, Curr. Protoc. Pharmacol. (2011). Chapter 14:Unit 14 16.
[30] Y. Yan, W. Jiang, Y. Tan, S. Zou, H. Zhang, F. Mao, A. Gong, et al., hucMSC exosome-derived GPX1 is required for the recovery of hepatic oxidant injury, Mol. Ther. 25 (2017) 465–479.
[31] H. Jiang, H. Zhao, M. Zhang, Y. He, X. Li, Y. Xu, X. Liu, Hypoxia induced changes of exosome Cargo and subsequent biological effects, Front. Immunol. 13 (2022), 824188.
[32] I. Dalle-Donne, R. Rossi, D. Giustarini, A. Milzani, R. Colombo, Protein carbonyl groups as biomarkers of oxidative stress, Clin. Chim. Acta 329 (2003) 23–38.
[33] Y. Gusev, K. Bhuvaneshwar, L. Song, J.C. Zenklusen, H. Fine, S. Madhavan, The REMBRANDT study, a large collection of genomic data from brain cancer patients, Sci. Data 5 (2018), 180158.
[34] C.H. Hsieh, H.T. Chang, W.C. Shen, W.C. Shyu, R.S. Liu, Imaging the impact of Nox4 in cycling hypoxia-mediated U87 glioblastoma invasion and infiltration, Mol. Imag. Biol. 14 (2012) 489–499.
[35] C.H. Hsieh, W.C. Shyu, C.Y. Chiang, J.W. Kuo, W.C. Shen, R.S. Liu, NADPH oxidase subunit 4-mediated reactive oxygen species contribute to cycling hypoxia-promoted tumor progression in glioblastoma multiforme, PLoS One 6 (2011), e23945.
[36] C.H. Hsieh, C.P. Wu, H.T. Lee, J.A. Liang, C.Y. Yu, Y.J. Lin, NADPH oxidase subunit 4 mediates cycling hypoxia-promoted radiation resistance in glioblastoma multiforme, Free Radic. Biol. Med. 53 (2012) 649–658.
[37] H. Li, C. Peng, C. Zhu, S. Nie, X. Qian, Z. Shi, M. Shi, et al., Hypoxia promotes the metastasis of pancreatic cancer through regulating NOX4/KDM5A-mediated histone methylation modification changes in a HIF1A-independent manner, Clin. Epigenet. 13 (2021) 18.
[38] M. Miyashita-Ishiwata, M. El Sabeh, L.D. Reschke, S. Afrin, M.A. Borahay, Hypoxia induces proliferation via NOX4-Mediated oxidative stress and TGF-beta3 signaling in uterine leiomyoma cells, Free Radic. Res. 56 (2022) 163–172.

[39] Z. Liu, K. Tu, Y. Wang, B. Yao, Q. Li, L. Wang, C. Dou, et al., Hypoxia accelerates aggressiveness of hepatocellular carcinoma cells involving oxidative stress, epithelial-mesenchymal transition and non-canonical Hedgehog signaling, Cell. Physiol. Biochem. 44 (2017) 1856–1868.
[40] J.P. Fitzgerald, B. Nayak, K. Shanmugasundaram, W. Friedrichs, S. Sudarshan, A. A. Eid, T. DeNapoli, et al., Nox4 mediates renal cell carcinoma cell invasion through hypoxia-induced interleukin 6- and 8- production, PLoS One 7 (2012), e30712.
[41] S. Gong, S. Wang, M. Shao, NADPH oxidase 4: a potential therapeutic target of malignancy, Front. Cell Dev. Biol. 10 (2022), 884412.
[42] G.Y. Liou, P. Storz, Reactive oxygen species in cancer, Free Radic. Res. 44 (2010) 479–496.
[43] D.B. Cowan, R.D. Weisel, W.G. Williams, D.A. Mickle, Identification of oxygen responsive elements in the 5'-flanking region of the human glutathione peroxidase gene, J. Biol. Chem. 268 (1993) 26904–26910.
[44] F. Merante, S.M. Altamentova, D.A. Mickle, R.D. Weisel, B.J. Thatcher, B. M. Martin, J.G. Marshall, et al., The characterization and purification of a human transcription factor modulating the glutathione peroxidase gene in response to oxygen tension, Mol. Cell. Biochem. 229 (2002) 73–83.
[45] Y. Zhao, H. Wang, J. Zhou, Q. Shao, Glutathione peroxidase GPX1 and its dichotomous roles in cancer, Cancers (Basel) 14 (2022).
[46] Y. Huang, W. Fang, Y. Wang, W. Yang, B. Xiong, Transforming growth factor-beta1 induces glutathione peroxidase-1 and protects from H2O2-induced cell death in colon cancer cells via the Smad2/ERK1/2/HIF-1alpha pathway, Int. J. Mol. Med. 29 (2012) 906–912.
[47] I. Dokic, C. Hartmann, C. Herold-Mende, A. Regnier-Vigouroux, Glutathione peroxidase 1 activity dictates the sensitivity of glioblastoma cells to oxidative stress, Glia 60 (2012) 1785–1800.
[48] X. Wang, M. Han, S. Wang, Y. Sun, W. Zhao, Z. Xue, X. Liang, et al., Targeting the splicing factor NONO inhibits GBM progression through GPX1 intron retention, Theranostics 12 (2022) 5451–5469.
[49] W. Yang, Y. Shen, J. Wei, F. Liu, MicroRNA-153/Nrf-2/GPx1 pathway regulates radiosensitivity and stemness of glioma stem cells via reactive oxygen species, Oncotarget 6 (2015) 22006–22027.
[50] H.L. Zeng, L. Hu, X. Chen, Q.Q. Han, H. Li, L. Cheng, C.X. Li, DIA-MS based proteomics combined with RNA-Seq data to unveil the mitochondrial dysfunction in human glioblastoma, Molecules 28 (2023).
[51] M. Lopez-Lazaro, Dual role of hydrogen peroxide in cancer: possible relevance to cancer chemoprevention and therapy, Cancer Lett. 252 (2007) 1–8.
[52] T. Chidawanyika, S. Supattapone, Hydrogen peroxide-induced cell death in mammalian cells, J Cell Signal 2 (2021) 206–211.
[53] M.P. Lisanti, U.E. Martinez-Outschoorn, Z. Lin, S. Pavlides, D. Whitaker-Menezes, R.G. Pestell, A. Howell, et al., Hydrogen peroxide fuels aging, inflammation, cancer metabolism and metastasis: the seed and soil also needs "fertilizer", Cell Cycle 10 (2011) 2440–2449.
[54] M. Garcia-Barros, F. Paris, C. Cordon-Cardo, D. Lyden, S. Rafii, A. Haimovitz-Friedman, Z. Fuks, et al., Tumor response to radiotherapy regulated by endothelial cell apoptosis, Science 300 (2003) 1155–1159.
[55] R.K. Jain, Normalization of tumor vasculature: an emerging concept in antiangiogenic therapy, Science 307 (2005) 58–62.
[56] K. Hida, N. Maishi, C. Torii, Y. Hida, Tumor angiogenesis–characteristics of tumor endothelial cells, Int. J. Clin. Oncol. 21 (2016) 206–212.
[57] D.H. Gorski, M.A. Beckett, N.T. Jaskowiak, D.P. Calvin, H.J. Mauceri, R. M. Salloum, S. Seetharam, et al., Blockage of the vascular endothelial growth factor stress response increases the antitumor effects of ionizing radiation, Cancer Res. 59 (1999) 3374–3378.
[58] F.R. Gonzalez-Pacheco, J.J. Deudero, M.C. Castellanos, M.A. Castilla, M.V. Alvarez-Arroyo, S. Yague, C. Caramelo, Mechanisms of endothelial response to oxidative aggression: protective role of autologous VEGF and induction of VEGFR2 by H2O2, Am. J. Physiol. Heart Circ. Physiol. 291 (2006) H1395–H1401.
[59] B.L. Krock, N. Skuli, M.C. Simon, Hypoxia-induced angiogenesis: good and evil, Genes Canc. 2 (2011) 1117–1133.
[60] T. Kamba, D.M. McDonald, Mechanisms of adverse effects of anti-VEGF therapy for cancer, Br. J. Cancer 96 (2007) 1788–1795.
[61] Y. Haibe, M. Kreidieh, H. El Hajj, I. Khalifeh, D. Mukherji, S. Temraz, A. Shamseddine, Resistance mechanisms to anti-angiogenic therapies in cancer, Front. Oncol. 10 (2020) 221.
[62] D.A. Reardon, S. Turner, K.B. Peters, A. Desjardins, S. Gururangan, J.H. Sampson, R.E. McLendon, et al., A review of VEGF/VEGFR-targeted therapeutics for recurrent glioblastoma, J. Natl. Compr. Cancer Netw. 9 (2011) 414–427.
[63] M. Karami Fath, J. Azami, A. Masoudi, R. Mosaddeghi Heris, E. Rahmani, F. Alavi, A. Alagheband Bahrami, et al., Exosome-based strategies for diagnosis and therapy of glioma cancer, Cancer Cell Int. 22 (2022) 262.
[64] X. Yue, F. Lan, T. Xia, Hypoxic glioma cell-secreted exosomal miR-301a activates Wnt/β-catenin signaling and promotes radiation resistance by targeting TCEAL7, Mol. Ther. 27 (2019) 1939–1949.
[65] C. Zhao, H. Wang, C. Xiong, Y. Liu, Hypoxic glioblastoma release exosomal VEGF-A induce the permeability of blood-brain barrier, Biochem. Biophys. Res. Commun. 502 (2018) 324–331.
[66] R. Wei, H. Qiu, J. Xu, J. Mo, Y. Liu, Y. Gui, G. Huang, et al., Expression and prognostic potential of GPX1 in human cancers based on data mining, Ann. Transl. Med. 8 (2020) 124.